

Noisy Data Meets Privacy: Training Local Models with Post-Processed Remote Queries

Kexin Li¹ Aastha Mehta² David Lie¹

¹University of Toronto ²The University of British Columbia

Abstract

The adoption of large cloud-based models for inference in privacy-sensitive domains, such as homeless care systems and medical imaging, raises concerns about end-user data privacy. A common solution is adding locally differentially private (LDP) noise to queries before transmission, but this often reduces utility. LDPKiT, which stands for *Local Differentially-Private and Utility-Preserving Inference via Knowledge Transfer*, addresses the concern by generating a privacy-preserving inference dataset aligned with the private data distribution. This dataset is used to train a reliable local model for inference on sensitive inputs. LDPKiT employs a two-layer noise injection framework that leverages LDP and its post-processing property to create a privacy-protected inference dataset. The first layer ensures privacy, while the second layer helps to recover utility by creating a sufficiently large dataset for subsequent local model extraction using noisy labels returned from a cloud model on privacy-protected noisy inputs. Our experiments on Fashion-MNIST, SVHN and PathMNIST medical datasets demonstrate that LDPKiT effectively improves utility while preserving privacy. Moreover, the benefits of using LDPKiT increase at higher, more privacy-protective noise levels. For instance, on SVHN, LDPKiT achieves similar inference accuracy with $\epsilon = 1.25$ as it does with $\epsilon = 2.0$, providing stronger privacy guarantees with less than a 2% drop in accuracy. Furthermore, we perform extensive sensitivity analyses to evaluate the impact of dataset sizes on LDPKiT’s effectiveness and systematically analyze the latent space representations to offer a theoretical explanation for its accuracy improvements. Lastly, we qualitatively and quantitatively demonstrate that the type of knowledge distillation performed by LDPKiT is ethical and fundamentally distinct from adversarial model extraction attacks.

1 Introduction

Many high-performance machine learning (ML) applications are trained and hosted by online services, which have better

access to large datasets and the computation necessary to train large models. However, users of such models may be concerned about the leakage of sensitive information in the queries they make to such cloud providers during inference, who could monitor or inspect their queries and use the information for purposes without their knowledge. Instances of providers misusing users’ data abound. In 2016, for example, Yahoo secretly complied with the US government’s digital communication surveillance and used its custom spam and child pornography detection system to monitor the user’s emails [1–3]. In 2022, the Amazon Ring Doorbell was found to have disclosed users’ video and audio footage to the police without authorization [4]. Even the recent large language models have incurred data leakage [5, 6], leading to many organizations banning their use. Even with a trusted model provider, a compromised cloud platform could enable an adversary to infer the user’s queries via side-channels [7].

Such concerns become even more acute in the domain of applications involving privacy-sensitive data, such as medical imaging [8], disease diagnosis [9], financial fraud detection [10], and systems supporting the vulnerable populations such as the homeless [11], which increasingly rely on machine learning automated decision making. Further, such domains may be challenged by a scarcity of publicly available training data, making it difficult for users to obtain and train reliable models of their own. For instance, when a person facing a crisis enquires for homeless care support, their personal status and needs information may be used to determine their eligibility for shelter, but their data should not be used for surveillance or targeting of vulnerable individuals. Similarly, in a medical imaging system, a patient’s sensitive data may be used for diagnostic purposes, but they might be concerned about their data being shared with insurance providers or potential employers.

Various methods for protecting privacy during inference have been proposed. For example, homomorphic encryption [12, 13] and hardware-enforced trusted execution environments [14] can help to protect users’ inference queries against a compromised cloud platform. However, they can-

not protect against a malicious or faulty model that may leak information about the inputs it is performing inference on.

An alternative approach that obtains strong privacy guarantees is to limit the amount of information that is sent to the model in a query. One way to limit the amount of information is to use a local differential privacy (LDP) based inference mechanism, which bounds the amount of information leakage by adding random noise to the query inputs before transmitting them for inference [15]. However, to obtain a reasonable guarantee of privacy, LDP requires a large amount of noise to be added to each input, leading to loss of utility [16].

In an ideal case, users could just train and use their own model locally, or a model provider could share the weights with a user enabling them to use the model locally. Such a model frees users from having to send any sensitive data to a model provider. However, in many specialized scenarios, it may be challenging for users to obtain the large, labelled training sets that are required to train highly accurate models. Similarly, in addition to economic motivations, model providers with models trained on private data may be reluctant to share their models with users out of concern about leaking the sensitive data in the model itself [17].

In this work, we propose, LDPKiT (*Local Differentially-Private and Utility-Preserving Inference via Knowledge Transfer*), which uses LDP to enable users to obtain a local model through knowledge transfer (*i.e.*, model extraction). A key challenge with model extraction is that the user requires a set of in-distribution data with which to query the model. We seek to address scenarios where the availability of public data in the same distribution as the user’s private data is scarce, thus forcing the user to use their own private data for extraction. Naïvely adding LDP to the data before querying introduces significant noise into the labels returned by the model, degrading the model extraction. LDPKiT overcomes this challenge by adding noise to each private input, and then *superimposing* pairs of the noised inputs with each other before querying them. This has the benefit of creating more in-distribution inputs, enabling efficient knowledge transfer from the model provider.

Model extraction can be a controversial technique. In the extreme case, malicious model extraction (*i.e.*, model theft), where an adversary extracts a model provider’s commercial model and then resells that model can cause economic harm to the model provider and disincentivize model providers from training or providing machine learning services. We naturally do not advocate such uses of model extraction. In contrast, our approach differs from this model theft in several important ways: 1) LDPKiT’s extracted model’s performance does not match the provider’s model due to the addition of LDP noise. As a result, the model extraction is not for competitive purposes, and would not violate the terms of service of most commercial model providers [18]—the main objective of LDPKiT’s model extraction is to protect user privacy. 2) Users still perform queries to the model provider, and pre-

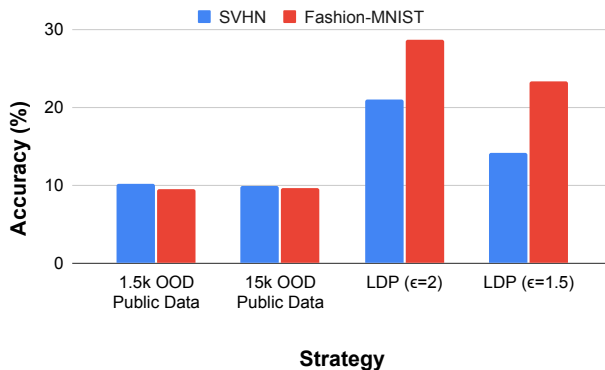


Figure 1: Comparison of accuracies: Training a local model (ResNet-18) with out-of-distribution (OOD) public data samples versus querying the cloud service model with ϵ -LDP protected private data samples.

sumably compensate the model provider for these queries. As preventing model extraction, especially for small models, is inherently challenging, it is often accounted for in query pricing structures [19–21]. We further discuss our ethical use of model extraction principles in detail in Section 6.1.

Our analysis is guided by the following research questions:

- RQ1.** Does LDPKiT recover the utility impacted by LDP noise? (Section 4.2)
- RQ2.** Why superimposition works in LDPKiT? (Section 4.3)
- RQ3.** How do the size of the private dataset and number of queries impact LDPKiT? (Section 4.4)

Contributions. LDPKiT generates inference datasets that are both privacy-protective and close to the distribution of sensitive datasets, allowing users to accurately annotate their private data with mitigated privacy concerns. We evaluate LDPKiT across diverse applications and multiple model architectures, systematically examining its performance and sensitivity to dataset sizes. Additionally, we conduct in-depth analyses of latent space representations to uncover the underlying factors contributing to LDPKiT’s effectiveness.

2 Overview

2.1 Target Scenario

Our target scenario is the use of privacy-sensitive ML cloud services. As discussed in Section 1, the ideal, but unrealistic, solution would be granting users access to cloud-hosted models for local deployment. Instead, users may opt to train their own models through knowledge transfer techniques. We target privacy-sensitive applications whose in-distribution public data is not readily available. As an illustration, we train two instances of ResNet-18 model with one of the two datasets,

SVHN and Fashion-MNIST, and subsequently run inference queries on each model using data from the dataset on which it was not trained. As shown in Figure 1, the model accuracy drops to the level of random guessing (*i.e.*, around 10% for 10-class datasets) when it is extracted using out-of-distribution (OOD) data samples (*e.g.*, SVHN samples are considered OOD for the Fashion-MNIST task, and vice versa). Instead of extracting a model from OOD samples and recording its accuracies, we focus on querying a model (*e.g.*, ResNet-152 in this experiment) trained on in-distribution data using queries derived from the same datasets but modified with LDP under highly privacy-protective ϵ settings. Even without any utility recovery techniques, the recorded accuracies based on the returned labels remain around 20% on average. This observation motivates the use of ϵ -LDP as a viable starting point in our privacy-preserving framework, which we further enhance with techniques to recover the accuracy loss from the LDP noise. Further details are provided in Section 3.

Our design goals are to protect sensitive user queries when using ML cloud services during inference time and to recover some accuracy loss due to privacy-protective LDP noise added to the queries. We assume the cloud model provider is honest but curious. It honestly answers the user’s queries but may record both the queries and their results to infer information about the user. To evaluate the framework in a more challenging scenario, we also restrict access to the cloud model by assuming that the cloud model returns hard labels only.

2.2 Preliminaries and General Setup

Throughout this paper, we use \mathcal{M}_R to denote the remote, cloud-hosted model and \mathcal{M}_L to denote the local model hosted by the user. We use $\mathcal{D}_{\text{priv}}$ to denote the sensitive dataset the user owns and wishes to protect. Note that $\mathcal{D}_{\text{priv}}$ can be a predefined or dynamically generated set of points. We denote the number of private data points (*i.e.*, size of $\mathcal{D}_{\text{priv}}$) as $|\mathcal{D}_{\text{priv}}|$. $\mathcal{D}_{\text{protected}}$ refers to the privacy-protected $\mathcal{D}_{\text{priv}}$ with a single layer of ϵ -LDP noise applied. It has the same size as $\mathcal{D}_{\text{priv}}$. The complete set of candidates derived from post-processing $\mathcal{D}_{\text{protected}}$ with LDPKiT is represented as $\mathcal{D}_{\text{cand}}$, with its size $|\mathcal{D}_{\text{cand}}|$ calculated as $|\mathcal{D}_{\text{priv}}| \cdot (|\mathcal{D}_{\text{priv}}| - 1)$. Detailed explanations regarding this process are provided in Section 3. Subsequently, the user can construct a $\mathcal{D}_{\text{infer}}$ by selecting candidate data points from $\mathcal{D}_{\text{cand}}$ to query \mathcal{M}_R for labels. These labels are used to train an \mathcal{M}_L to annotate $\mathcal{D}_{\text{priv}}$. The size of $\mathcal{D}_{\text{infer}}$ ($|\mathcal{D}_{\text{infer}}|$), representing the number of queries made, is determined by the user, with a maximum possible size of $|\mathcal{D}_{\text{cand}}| = |\mathcal{D}_{\text{priv}}| \cdot (|\mathcal{D}_{\text{priv}}| - 1)$. We use *SIDP* to denote the process of the standard inference scheme with LDP where a single layer of noise is added to $\mathcal{D}_{\text{priv}}$ to form $\mathcal{D}_{\text{protected}}$. The user then queries \mathcal{M}_R using $\mathcal{D}_{\text{protected}}$ to obtain labels, which may include some errors due to the privacy-protective noise in the queries. In the *SIDP* method, the user straightforwardly accepts the potentially erroneous labels pro-

vided by \mathcal{M}_R without further post-processing. For instance, the LDP approach with results illustrated in the two rightmost scenarios of Figure 1 represents an *SIDP* usage. Although *SIDP* is promising in privacy preservation, it degrades utility significantly. Instead of accepting the errors, we propose two ways to post-process $\mathcal{D}_{\text{protected}}$ used in *SIDP* for our accurate privacy-preserving inference mechanism. We denote them as *LDPKiT-Rand* and *LDPKiT-Sup*. The details are discussed in Section 3.

2.3 Privacy Guarantee

LDPKiT ensures the privacy of $\mathcal{D}_{\text{priv}}$ during inference by applying LDP noise to each data sample. This section discusses the key concepts and methodologies essential for designing effective privacy-preserving noise mechanisms.

Definition 2.1. ϵ -Local Differential Privacy (LDP). We define ϵ -LDP as follows [22]: A randomized algorithm \mathcal{A} satisfies ϵ -LDP if for all pairs of values and all sets S of possible outputs, where $S \subseteq \text{Range}(\mathcal{A})$,

$$\Pr[\mathcal{A}(v_1) \in S] \leq e^\epsilon \Pr[\mathcal{A}(v_2) \in S] \quad (1)$$

A lower ϵ value indicates a tighter bound of the equation and a stronger privacy guarantee. As for the choice of random noise, we apply Laplacian noise to satisfy the ϵ -LDP privacy guarantee and the definition is as follows.

Definition 2.2. Laplacian Mechanism. The Laplacian mechanism of LDP adds noise drawn from the Laplacian distribution, with the probability density function (PDF) defined as follows for a variable z and a scaling factor $\lambda \propto \frac{1}{\epsilon}$:

$$L(z, \lambda) = \frac{1}{2\lambda} \exp\left(-\frac{|z|}{\lambda}\right) \quad (2)$$

For the design of the candidate dataset used for inference, $\mathcal{D}_{\text{cand}}$, we also leverage LDP’s post-processing property to facilitate utility recovery. If an algorithm safeguards an individual’s privacy, a data analyst cannot compromise privacy—whether under the formal definition or in any intuitive sense—merely by reflecting on the algorithm’s output [23]. Post-processing is commonly used in DP schemes to improve the interpretability or accuracy of differentially-private data [24]. The formal definition is as follows:

Definition 2.3. Post-Processing Property in ϵ -LDP. The post-processing property [23] of LDP states that if a randomized algorithm \mathcal{A} satisfies ϵ -LDP, then for any deterministic or randomized function g , the composed mechanism $g(\mathcal{A}(\cdot))$ also satisfies ϵ -LDP. Specifically, for all v_1, v_2 and for all subsets $\mathcal{T} \subseteq \text{Range}(g(\mathcal{A}))$, we have:

$$\Pr[g(\mathcal{A}(v_1)) \in \mathcal{T}] \leq e^\epsilon \Pr[g(\mathcal{A}(v_2)) \in \mathcal{T}]. \quad (3)$$

Post-processing immunity guarantees that applying function g to the output of \mathcal{A} does not compromise the privacy guarantees provided by ϵ -LDP.

We prove that LDPKiT’s noise injection scheme satisfies the definition of ϵ -LDP with the Laplacian mechanism in Appendix A.

3 Design

Figure 2 presents the system overview of LDPKiT, which has four main stages: I. post-processing on noise-injected $\mathcal{D}_{\text{protected}}$ to form $\mathcal{D}_{\text{infer}}$ for querying, II. cloud model inference with post-processed privacy-protected data in $\mathcal{D}_{\text{infer}}$, III. local training with inference results from \mathcal{M}_{R} and $\mathcal{D}_{\text{infer}}$, and IV. execution of users’ private inference queries on the local model with $\mathcal{D}_{\text{priv}}$. SIDP, on the other hand, does not involve model training. It queries \mathcal{M}_{R} with single-layer LDP noised data points and accepts \mathcal{M}_{R} ’s outputs directly. Prior to querying \mathcal{M}_{R} for inference, LDPKiT creates $\mathcal{D}_{\text{protected}}$ based on $\mathcal{D}_{\text{priv}}$ by adding random noise provable by the Laplacian mechanism (*i.e.*, SIDP). Subsequently, LDPKiT generates $\mathcal{D}_{\text{cand}}$ from $\mathcal{D}_{\text{protected}}$ by leveraging the post-processing property of ϵ -LDP [23]. The user has the flexibility to construct $\mathcal{D}_{\text{infer}}$ for \mathcal{M}_{R} inference from $\mathcal{D}_{\text{cand}}$ using methods such as random selection. For larger datasets, more advanced machine learning techniques, such as active learning [25] and core-set strategies [26], can be employed to optimize the query selection process. Once \mathcal{M}_{R} returns inference results, LDPKiT enters the local training stage. We train \mathcal{M}_{L} on pairs of the $\mathcal{D}_{\text{infer}}$ and \mathcal{M}_{R} ’s outputs, aiming to make \mathcal{M}_{L} achieve satisfactory accuracy on the original (noise-free) $\mathcal{D}_{\text{priv}}$. This approach enables LDPKiT to preserve inference utility while safeguarding the privacy of $\mathcal{D}_{\text{priv}}$ from \mathcal{M}_{R} . LDPKiT can also be applied to an online learning setting where the user can iterate through the entire process and periodically train \mathcal{M}_{L} using \mathcal{M}_{R} ’s predictions on new inference queries.

3.1 Preliminary Experiments

As demonstrated in Section 2.1, model extraction with OOD public data is ineffective. To perform successful model extraction that enables the user to annotate their private data locally on a trustworthy platform, our intuition is to use samples that are in-distribution with $\mathcal{D}_{\text{priv}}$ to query \mathcal{M}_{R} , while maintaining privacy through ϵ -LDP. One way is to add ϵ -LDP noise to in-distribution $\mathcal{D}_{\text{priv}}$ (*i.e.*, $\mathcal{D}_{\text{protected}}$). However, the limited size of $\mathcal{D}_{\text{protected}}$ is insufficient for model training. Hence, we need to find a way to generate additional data points to form $\mathcal{D}_{\text{cand}}$ from $\mathcal{D}_{\text{priv}}$ that protects privacy in $\mathcal{D}_{\text{priv}}$ while preserving a distribution as close to $\mathcal{D}_{\text{priv}}$ as possible.

We test our intuition by systematically introducing random noise to query samples. We employ a two-layer noise injection mechanism. First, we add a base layer of ϵ -LDP noise to each original private data sample, the same way as SIDP. In addition, we apply an additional layer of ϵ -LDP random noise as a post-processing step. Then, we use the post-processed

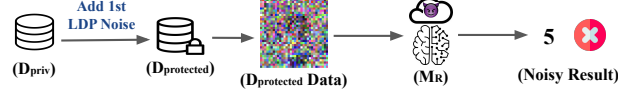
noisy data samples as queries for inference on \mathcal{M}_{R} . We describe two mechanisms for applying the second layer of ϵ -LDP noise in the next section. Further, we train the \mathcal{M}_{L} model on the post-processed noisy samples labelled by the \mathcal{M}_{R} . This approach enhances the \mathcal{M}_{L} ’s prediction accuracy beyond that of the \mathcal{M}_{R} over repeated queries while ensuring consistent privacy guarantees. The base noise remains intact throughout the querying process, and the post-processing of the noised private samples complies with the post-processing property of LDP. A detailed proof of the privacy guarantees is provided in Appendix A.

To realize our idea, we conduct a proof-of-concept experiment on Fashion-MNIST. Specifically, we construct a relatively small $\mathcal{D}_{\text{priv}}$ with 500 samples randomly selected from Fashion-MNIST. We set \mathcal{M}_{R} as ResNet-152 and \mathcal{M}_{L} as ResNet-18. To ensure robust and reliable results, we average the accuracies over three runs and across three different dataset splits, mitigating the influence of randomness. We calibrate the ϵ value to 2.0 so that \mathcal{M}_{R} ’s inference accuracy under SIDP (with a single layer of noise applied to each data point) is only a few multiples of the probability of random guessing (*e.g.*, 15% to 30%). This configuration ensures that \mathcal{M}_{R} provides minimal yet sufficient information while preserving privacy. The recorded SIDP accuracy is 29.86%. We then implement and evaluate our above-mentioned two-layer noise injection mechanism. We post-process 500 SIDP queries with an extra layer of random noise to form an inference dataset, $\mathcal{D}_{\text{infer}}$ with 249,500 data points (*i.e.*, its maximum available dataset size with 499 randomly noised variations of the SIDP noisy queries). We then train \mathcal{M}_{L} with $\mathcal{D}_{\text{infer}}$ and \mathcal{M}_{R} ’s noisy predictions on those noisy data. The trained \mathcal{M}_{L} ’s inference accuracy on the 500 original (noise-free) $\mathcal{D}_{\text{priv}}$ samples is improved to 43.56% (*i.e.*, 13% accuracy increase compared to SIDP) without compromising the privacy level. We collect the p value results from the dependent two-sample t-test for statistical significance and the value is negligible; hence, the improvement is solid. However, the utility recovery achieved through this mechanism does not yield an optimal trade-off between utility and privacy. One reason is that $\mathcal{D}_{\text{priv}}$ is too small (*i.e.*, 500 data samples). More importantly, the idea of post-processing the noised private data with an extra layer of random noise is intuitive yet undirected. Thus, we further investigate whether more advanced strategies can be devised to design the post-processing LDP noise applied to $\mathcal{D}_{\text{priv}}$ in forming $\mathcal{D}_{\text{infer}}$, enabling the \mathcal{M}_{L} to learn more meaningful information about the decision boundaries and achieve improved accuracy. We elaborate on our design of LDP noise in Section 3.2 and discuss the results in Section 4.

3.2 LDPKiT’s Noise Injection Mechanism

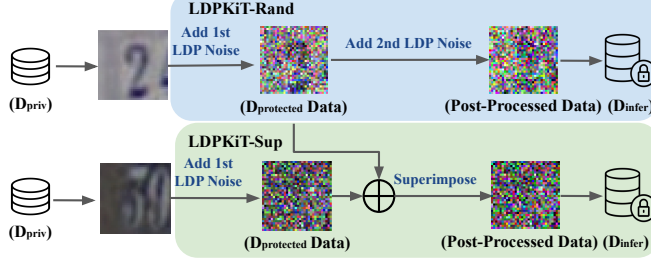
LDPKiT applies Laplacian noise to the privacy-sensitive queries in $\mathcal{D}_{\text{priv}}$ to generate $\mathcal{D}_{\text{infer}}$ for cloud model inference, ensuring the ϵ -LDP guarantee [22]. We define ϵ in the con-

SIDP: Remote Inference and Accept the Outputs

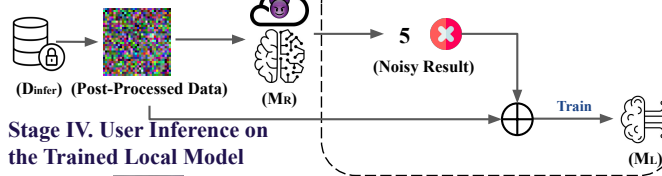


LDPKiT: Local Training with Post-Processed Data

Stage I. Noise Injection with Post-Processing



Stage II. Remote Inference



Stage III. LDPKiT Local Training

Stage IV. User Inference on the Trained Local Model

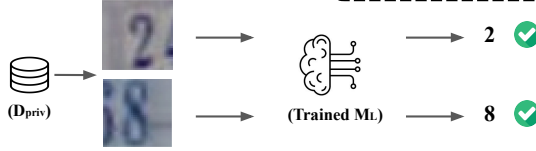


Figure 2: LDPKiT system overview.

text of LDP; therefore, the same amount of noise is added to each data sample in $\mathcal{D}_{\text{priv}}$ based on the ϵ value. We assume that queries in $\mathcal{D}_{\text{priv}}$ are independent and identically distributed (*i.i.d.*), and the formulation of ϵ -LDP is valid for each individual data point in $\mathcal{D}_{\text{priv}}$. Consequently, the privacy leakage is non-cumulative and bounded by ϵ per query. Given a private dataset $\mathcal{D}_{\text{priv}}$ containing $|\mathcal{D}_{\text{priv}}|$ *i.i.d.* data points, our goal is to create a $\mathcal{D}_{\text{infer}}$ dataset for querying \mathcal{M}_R and training \mathcal{M}_L with privacy safeguarded by ϵ -LDP. To achieve this, we employ a two-layer noise injection framework. We first add Laplacian noise with a scale inversely proportional to ϵ to each data point $d_{\text{priv}_i} \in \mathcal{D}_{\text{priv}}$ to form $\mathcal{D}_{\text{protected}}$ with the same size as $\mathcal{D}_{\text{priv}}$, where $i = 1, 2, \dots, |\mathcal{D}_{\text{priv}}|$. This first layer of base Laplacian noise remains intact throughout the entire post-processing and inference process for privacy protection. Then, unlike the conventional use of differentially private Laplacian noise (*i.e.*, SIDP), LDPKiT applies the second layer of noise to $\mathcal{D}_{\text{protected}}$ adhering to the post-processing property in two alternative ways. This layer of noise aims to expand the $\mathcal{D}_{\text{infer}}$ for knowledge transfer and recovering the labels of $\mathcal{D}_{\text{priv}}$. Details are described as follows.

Addition of an extra layer of random noise that satisfies ϵ -LDP (LDPKiT-Rand). As a baseline approach, we apply post-processing to each data point in $\mathcal{D}_{\text{protected}}$ by adding an additional layer of Laplacian noise (L) with the same scale

in the form of $d_{\text{cand}_i} \in \mathcal{D}_{\text{cand}} = d_{\text{priv}_i} \in \mathcal{D}_{\text{priv}} + L_1 + L_2$ for $i = 1, 2, \dots, |\mathcal{D}_{\text{priv}}|$. Although theoretically, we can generate an infinite number of random versions of each $\mathcal{D}_{\text{protected}}$ data point to construct $\mathcal{D}_{\text{cand}}$, we cap the final dataset $\mathcal{D}_{\text{cand}}$ to have at most $|\mathcal{D}_{\text{priv}}| \cdot (|\mathcal{D}_{\text{priv}}| - 1)$ data points, aligning with the second mechanism in the next section for evaluation purposes.

Superimposition of other noised data points in $\mathcal{D}_{\text{infer}}$ that also satisfies ϵ -LDP (LDPKiT-Sup). LDPKiT-Rand introduces unrelated noise that may cause the resulting data to deviate further from the distribution of $\mathcal{D}_{\text{priv}}$. To address this and generate more in-distribution samples, we adopt a different approach designed to better preserve the characteristics of $\mathcal{D}_{\text{priv}}$. After applying the first layer of ϵ -LDP random noise to each data point in $\mathcal{D}_{\text{priv}}$, we exhaustively combine these modified data points in all possible pairs with averaged pixel-wise addition. The candidate data point $d_{\text{cand}_i} \in \mathcal{D}_{\text{cand}}$ is computed as $d_{\text{cand}_i} = (d_{\text{protected}_i} + d_{\text{protected}_j})/2, i, j = 1, 2, \dots, |\mathcal{D}_{\text{priv}}|$. This process results in at most $|\mathcal{D}_{\text{priv}}| \cdot (|\mathcal{D}_{\text{priv}}| - 1)$ distinct permutations in the protected candidate dataset $\mathcal{D}_{\text{cand}}$.

When querying \mathcal{M}_R with $\mathcal{D}_{\text{infer}}$, the user has the option to utilize either the entire available dataset ($\mathcal{D}_{\text{cand}}$) or a randomly selected subset of it. We analyze the effect of the size of $\mathcal{D}_{\text{infer}}$ ($|\mathcal{D}_{\text{infer}}|$) in Section 4.4. In Appendix A, we prove that the post-processed noisy data points in the final inference dataset $\mathcal{D}_{\text{infer}}$, generated using both LDPKiT-Rand and LDPKiT-Sup,

adhere to ϵ -LDP and satisfy the post-processing property of LDP.

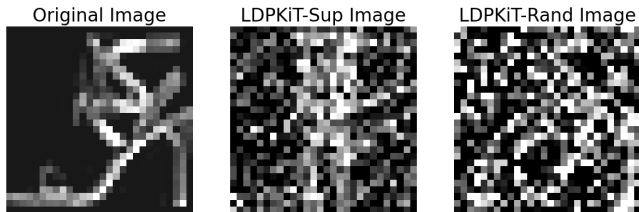


Figure 3: Sample of a noised Fashion-MNIST data point with label 5 (sandal) and ϵ set to 1.5.

4 Evaluation

In this section, we discuss the evaluation results and answer our research questions in Section 1 with empirical analysis.

4.1 Experimental setup

We run our experiments on two machines. One has two GPUs, NVIDIA GeForce RTX 3090 and 4090, with 24GB of dedicated memory, and an Intel 12th Gen i7-12700 CPU with 12 cores and 64GB of RAM. The other has two NVIDIA GeForce RTX 4090 GPUs and an AMD Ryzen Threadripper PRO 5955WX CPU with 16 cores and 64GB of RAM. The underlying OS are 64-bit Ubuntu 22.04.3 LTS and Ubuntu 24.04 LTS, respectively. We use Python 3.9.7 and PyTorch v2.1.2 with CUDA 12.1.

We evaluate LDPKiT on three diverse datasets, namely SVHN [27], Fashion-MNIST [28] and PathMNIST from MedMNIST2D for medical imaging in pathology [29]. For the ML models, we use ResNet-152 [30] as \mathcal{M}_R , and ResNet-18 [30] and MobileNetV2 [31] as \mathcal{M}_L . We assume that \mathcal{M}_R only returns the hard labels. The \mathcal{M}_L models are initialized with random weights. As a reference, when no privacy protection exists and thus no noise is added, \mathcal{M}_R 's average accuracies on \mathcal{D}_{priv} of Fashion-MNIST, SVHN and PathMNIST are 93.33%, 94.73% and 86.2%, respectively. The accuracies on an unseen validation dataset, \mathcal{D}_{val} , are 93.22%, 96.30% and 81.24%, respectively.

We construct different \mathcal{M}_R for different tasks and datasets. To allocate data points for \mathcal{D}_{priv} , instead of using the default training split, we train ResNet-152 (\mathcal{M}_R) on 35k, 48,257 and 89,996 data points for Fashion-MNIST, SVHN and PathMNIST, respectively. For Fashion-MNIST, the candidate pool of \mathcal{D}_{priv} has 25k data points with \mathcal{D}_{val} comprising 10k. For SVHN, the candidate pool for \mathcal{D}_{priv} is 25k and \mathcal{D}_{val} has 26,032 data points. For PathMNIST, the candidate pool for \mathcal{D}_{priv} has 10,004 data points and \mathcal{D}_{val} has 7,180. To simulate a scenario aligned with our setting, where users have limited private data requiring label information, we set $|\mathcal{D}_{priv}| = 1,500$ for

experiments in Sections 4.2 and 4.5. Specifically, we construct \mathcal{D}_{priv} by randomly selecting 1,500 balanced data points from the candidate pool to mitigate potential uncertainties associated with class imbalances. The effect of varying sizes of \mathcal{D}_{infer} and \mathcal{D}_{priv} is studied in Section 4.4. All experiments are repeated over three random seeds on three random subset splits to determine the statistical significance of our findings. The results of the dependent two-sample t-test confirm that all improvements are statistically significant (*i.e.*, $p < 0.05$).

We record SIDP accuracy based on the labels returned by \mathcal{M}_R for $\mathcal{D}_{protected}$, whereas LDPKiT accuracy is determined based on labels from \mathcal{M}_L for \mathcal{D}_{priv} where \mathcal{M}_L is trained on \mathcal{M}_R 's labels on \mathcal{D}_{infer} . To calibrate ϵ values per dataset, we ensure that the SIDP accuracy of \mathcal{M}_R corresponds to 1.5 – 3X random guessing (*e.g.*, 15% to 30% accuracy for a 10-class dataset), allowing \mathcal{M}_R to provide minimal but meaningful information for training \mathcal{M}_L . Specifically, we use ϵ values of 2.0, 1.5, and 1.25 for SVHN, 2.0 and 1.5 for Fashion-MNIST, and 10.0 and 7.0 for PathMNIST. Figure 3 shows a privacy-protected data point in Fashion-MNIST's \mathcal{D}_{cand} generated with LDPKiT-Rand and LDPKiT-Sup. Additional noisy samples are included in Appendix C. Details of our hyperparameter choices are discussed and reported in Appendix B.

4.2 RQ1: LDPKiT's Utility Recovery on \mathcal{D}_{priv}

In this section, we evaluate whether LDPKiT improves prediction accuracy on \mathcal{D}_{priv} compared to directly using \mathcal{M}_R 's noisy labels on $\mathcal{D}_{protected}$ (*i.e.*, SIDP). To simulate a realistic scenario, we set $|\mathcal{D}_{priv}|$ to 1,500, representing a practical data size a user might own. The entire \mathcal{D}_{cand} is used as \mathcal{D}_{infer} to minimize variations from random subset splits. To answer RQ1 quantitatively, we record the final accuracies of \mathcal{M}_L on the original \mathcal{D}_{priv} at the last epoch of training and \mathcal{M}_R 's SIDP accuracies on $\mathcal{D}_{protected}$. We compare the performance of SIDP and LDPKiT with different noise generation mechanisms in Figures 4 and 5. We also tabulate the numerical accuracies on \mathcal{D}_{priv} and \mathcal{D}_{val} in Tables 5, 6 and 7 in Appendix D.1. The results demonstrate that the extracted \mathcal{M}_L with LDPKiT, regardless of the noise generation mechanism, can almost always achieve higher prediction accuracies on \mathcal{D}_{priv} compared to SIDP. For instance, when $\epsilon = 2.0$, ResNet-152 (\mathcal{M}_R)'s SIDP accuracy on SVHN is only 21.07%, whereas both LDPKiT-Rand and LDPKiT-Sup can recover the inference accuracy of the trained ResNet-18 (\mathcal{M}_L) to approximately 85%. However, the improvement is not always significant and largely depends on the specific noise generation mechanism of LDPKiT. When employing LDPKiT-Rand, ResNet-18 achieves only 68.52% and 58.07% accuracy on Fashion-MNIST with ϵ values of 2.0 and 1.5, respectively, and MobileNetV2's accuracies fall below 60%. On PathMNIST, ResNet-18's performance is also inadequate, and MobileNetV2's accuracy with LDPKiT-Rand is even lower than SIDP.

From the two right-most bars in each column of Figures 4

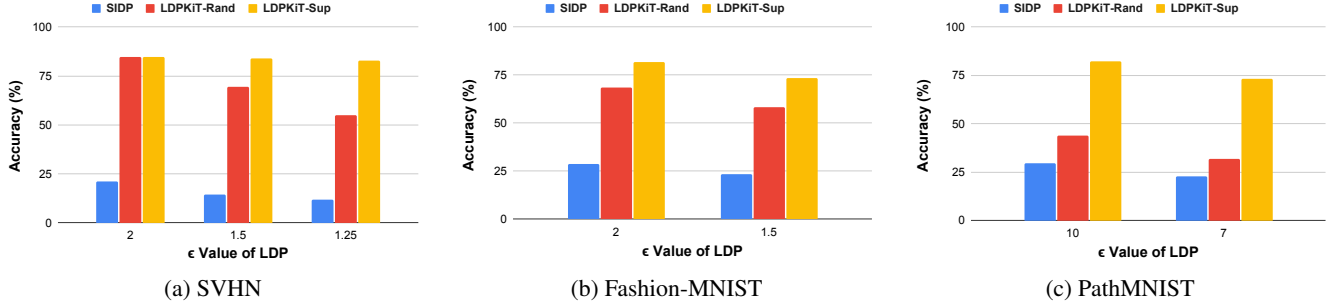


Figure 4: Accuracy comparisons on $\mathcal{D}_{\text{priv}}$ with calibrated ϵ values: SIDP versus ResNet-18(\mathcal{M}_L) trained using LDPKiT-Rand and LDPKiT-Sup.

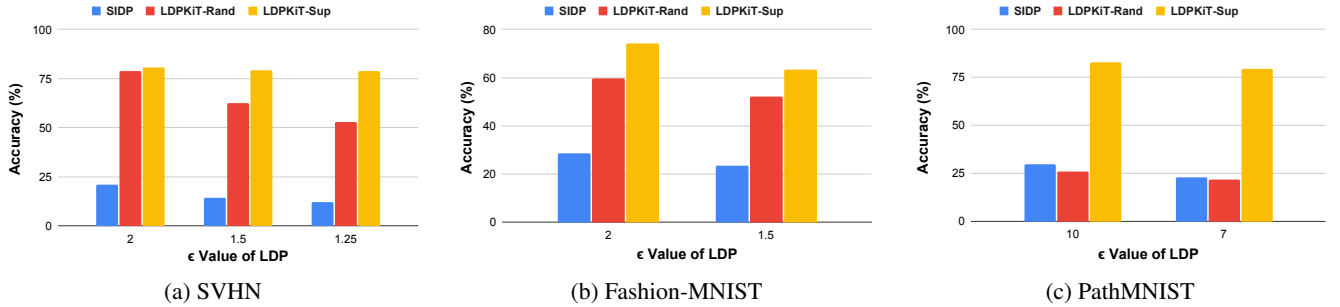


Figure 5: Accuracy comparisons on $\mathcal{D}_{\text{priv}}$ with calibrated ϵ values: SIDP versus MobileNetV2(\mathcal{M}_L) trained using LDPKiT-Rand and LDPKiT-Sup.

and 5, we also observe that the local models learn more effectively from $\mathcal{D}_{\text{infer}}$ created by superimposing noised data points within $\mathcal{D}_{\text{priv}}$, *i.e.*, LDPKiT-Sup, rather than applying arbitrary random noise as in LDPKiT-Rand. For instance, LDPKiT-Sup improves ResNet-18’s accuracy to 81.78% on Fashion-MNIST when ϵ is 2.0, compared to 28.69% with SIDP and 68.52% with LDPKiT-Rand. Similarly, ResNet-18’s accuracy is recovered to 82.11% on PathMNIST when ϵ is 10.0, far exceeding the 28.74% SIDP and 43.90% LDPKiT-Rand accuracies. Furthermore, we notice that ResNet-18 and MobileNetV2’s inference accuracies are consistently over or around 80% on SVHN when SIDP accuracy ranges between 11.87% and 21.07%. This demonstrates that LDPKiT-Sup can provide better privacy with essentially minimal loss of accuracy. Overall, the experimental results confirm that LDPKiT effectively recovers most of the utility loss caused by LDP noise under strictly privacy-preserving noise levels.

Note that the base noise and post-processing noise in LDPKiT-Rand are set to the same noise level (*i.e.*, ϵ value) by default, as described in Section 3.2. While it may seem intuitive to adjust LDPKiT-Rand by lowering the noise level of the post-processing layer (*i.e.*, increasing ϵ for the second layer of noise) to achieve higher accuracy, empirical results suggest that maintaining the same ϵ value for the post-processing noise as the base noise is more efficient and accuracy-preserving. To explore the optimal setting of

LDPKiT-Rand, we test on SVHN with ResNet-18 (\mathcal{M}_L), setting base noise ϵ_1 to 1.5 and 1.25 with varying ϵ_2 for post-processing noise. In Figure 6, the left-most green bar represents LDPKiT-Sup’s inference accuracy, showing consistent outperformance of LDPKiT-Rand regardless of ϵ combinations. The orange bar indicates LDPKiT-Rand’s accuracy when $\epsilon_1 = \epsilon_2$. The results reveal that deviating the post-processing noise significantly from the base noise reduces LDPKiT-Rand’s utility. Although it seems like $\epsilon_2 = 2.0$ exhibits the optimal accuracy, it is worth noting that the combinations of $\epsilon_1 = 1.5, \epsilon_2 = 2.0$ and $\epsilon_1 = 1.25, \epsilon_2 = 2.0$ both achieve lower accuracies than the 84.86% obtained when $\epsilon_1 = \epsilon_2 = 2.0$ (See Figure 4b). It is also empirically challenging for the user to determine the second ϵ before inference. Therefore, aligning the ϵ of the post-processing noise with the base noise is recommended for optimal efficiency and practicality.

4.3 RQ2: Latent Space Analysis

In Section 4.2, we quantitatively demonstrate that LDPKiT enhances inference accuracy on $\mathcal{D}_{\text{priv}}$ compared to SIDP, with LDPKiT-Sup consistently outperforming the LDPKiT-Rand noise generation algorithms. We empirically demonstrate that ML models trained with LDPKiT-Sup—including ResNet-18 and MobileNetV2—achieve higher accuracies on $\mathcal{D}_{\text{priv}}$ and

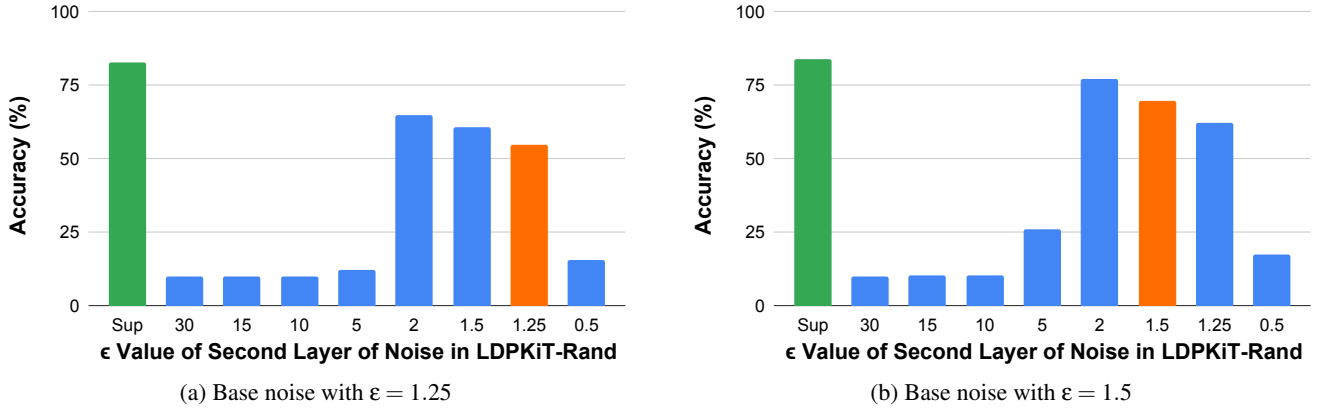


Figure 6: Comparison of LDPKiT-Rand’s inference accuracies with different ϵ values for the post-processing layer of LDP noise versus LDPKiT-Sup.

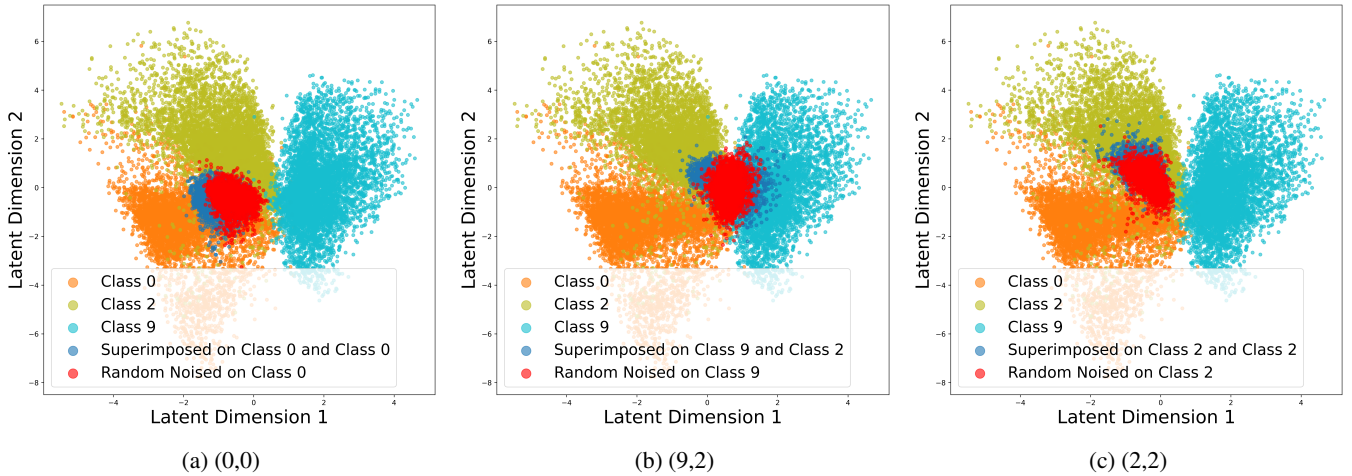


Figure 7: Latent space plots of Fashion-MNIST class triplets (C0-T-shirt/top, C2-pullover, C9-ankle boot) and privacy-protected noisy data clusters generated with LDPKiT-Rand and LDPKiT-Sup ($\epsilon = 2.0$).

Table 1: Euclidean distances between centroids of clusters shown in Figure 7 on Fashion-MNIST.

Figure	Strategy	Class(es)	$d(C_N, C_0)$	$d(C_N, C_2)$	$d(C_N, C_9)$
7a	LDPKiT-Sup	(0,0)	1.9835	2.5191	3.2017
	LDPKiT-Rand	0	2.1195	2.4666	2.9169
7b	LDPKiT-Sup	(9,2)	3.1652	2.3538	2.0524
	LDPKiT-Rand	9	3.0937	2.5595	1.9333
7c	LDPKiT-Sup	(2,2)	2.9662	1.7351	2.9171
	LDPKiT-Rand	2	2.7084	1.9433	2.7115

$d(C_N, C_X)$ is the Euclidean distance between the centroids of the noisy data cluster and the Class X cluster.

\mathcal{D}_{val} than with LDPKiT-Rand. However, it is less apparent why LDPKiT-Sup is better than LDPKiT-Rand qualitatively. We hypothesize that the synthetic data points generated by

Table 2: Frequency with which LDPKiT-Rand is more divergent from the target class triplets compared to LDPKiT-Sup.

Dataset	Number of triplets with $DR > 1.0$	Total number of triplets	Frequency
SVHN	49	72	68.06%
Fashion-MNIST	25	36	69.44%
PathMNIST	15	22	68.18%

DR refers to the KL Divergence Ratio introduced in Section 4.3 Definition 4.2. Frequency refers to how often LDPKiT-Rand’s cluster is further from the target triplet cluster than LDPKiT-Sup (*i.e.*, LDPKiT-Sup’s cluster is closer to target distribution).

LDPKiT-Sup are closer to the distribution of the original data points from target classes compared to LDPKiT-Rand, enabling more effective knowledge transfer about how \mathcal{M}_R

Table 3: Sensitivity Analysis on $|\mathcal{D}_{\text{priv}}|$ and $|\mathcal{D}_{\text{infer}}|$ with ResNet-18 (\mathcal{M}_L).

Dataset	ϵ	LDPKiT	Accuracy on $\mathcal{D}_{\text{priv}}$ (%)															
			$ \mathcal{D}_{\text{priv}} $	125			250			500			1k			1.5k		
			$ \mathcal{D}_{\text{infer}} $	15,500	15,500	62,250	15,500	62,250	250k	15,500	62,250	250k	500k	15,500	62,250	250k	500k	
Fashion-MNIST	2.0	Rand	14.76	18.36	36.40	17.71	32.47	52.93	18.06	34.45	57.90	63.37	14.81	34.68	57.20	64.66		
		Sup	25.87	28.93	31.42	24.20	37.64	52.95	25.11	47.18	66.48	73.66	25.14	45.08	68.98	74.35		
SVHN	1.5	Rand	8.80	11.40	6.90	9.40	6.93	34.07	10.45	9.85	35.33	51.31	10.43	10.03	32.81	48.59		
		Sup	9.07	9.73	12.67	10.13	15.33	45.69	10.20	19.97	60.10	69.08	10.09	14.31	62.10	76.88		
Path-MNIST	10.0	Rand	24.36	24.80	29.87	22.89	32.78	44.40	24.48	30.81	50.40	43.37	23.56	29.00	43.73	54.39		
		Sup	41.07	41.42	47.51	44.00	54.98	69.93	40.93	48.49	73.33	76.97	42.99	57.20	74.14	76.79		

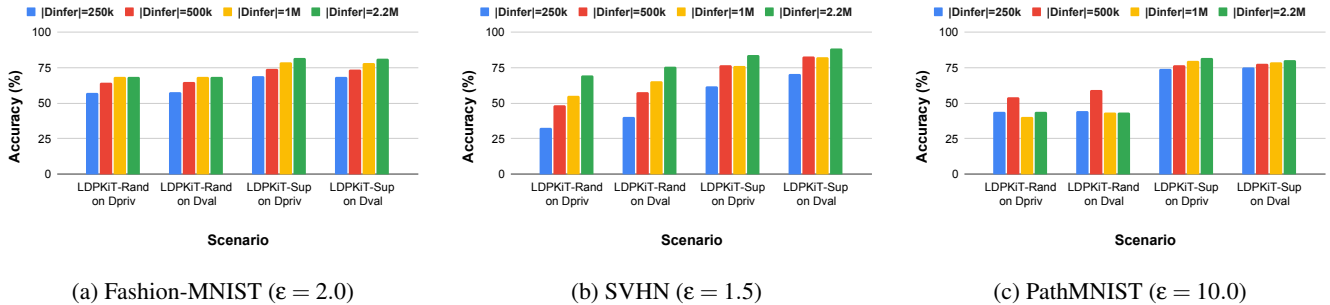


Figure 8: Comparison of ResNet18 (\mathcal{M}_L)’s accuracies on $\mathcal{D}_{\text{priv}}$ and \mathcal{D}_{val} with $|\mathcal{D}_{\text{priv}}| = 1.5k$ and various $|\mathcal{D}_{\text{infer}}|$.

classifies points in the latent space, including potentially better extraction of the decision boundaries. To evaluate our hypothesis, we plot and analyze the latent space of $\mathcal{D}_{\text{infer}}$. To replicate our framework in latent space, we first train a variational auto-encoder (VAE) on the data samples with ϵ -LDP noise from three random classes of the datasets. We pick ϵ values of 2.0 for Fashion-MNIST and SVHN, and 7.0 for PathMNIST. Other hyperparameter choices are discussed in Appendix B. Our training objective is to visualize three distinct clusters representing the original noise-free data samples corresponding to the three target classes. To achieve this, we replace the conventional reconstruction loss with the triplet margin loss. Using the trained VAE model, we further generate and visualize two additional clusters: noisy samples produced by LDPKiT-Sup based on two of the three classes, and noisy samples produced by LDPKiT-Rand based on one class. We then compute the Euclidean distances from these noisy clusters (*i.e.*, LDPKiT-Rand and LDPKiT-Sup) to the clean class clusters. This analysis allows us to evaluate whether LDPKiT-Sup offers a learning advantage over LDPKiT-Rand, particularly through the perspective of the latent space representation.

Figure 7 presents an example of Fashion-MNIST’s latent space visualization. Clusters of Class 0, Class 2 and Class 9 represent the original (noise-free) data points from those target classes. For instance, the cluster superimposed on Class 9 and Class 2 contains noised superimposed data points gener-

ated with LDPKiT-Sup from Class 2 and Class 9. The cluster randomized on Class 0 shows noised data points generated with LDPKiT-Rand on the target Class 0. The key observation is that the data distribution of the noisy cluster created with LDPKiT-Sup is closer to the distribution of the target class(es) than that of LDPKiT-Rand. For instance, LDPKiT-Sup’s cluster is closer to the cluster of the target class (*i.e.*, Class 0 or Class 2) than LDPKiT-Rand’s cluster in Figure 7a and Figure 7c. In Figure 7b, LDPKiT-Sup’s cluster is more spread out and has more overlapping area with the clusters of Class 2 and Class 9, whereas LDPKiT-Rand’s cluster remains more static and less representative, sitting in the middle of the clusters of Class 0, 2 and 9. Additional latent space analyses for triplet examples across other datasets are provided in Appendix D.4.

Table 1 provides the numerical Euclidean distances between the centroids of each cluster pairs from Figure 7. Here, the distance values further validate the observations from the plots. We note, however, that the Euclidean distance between centroids is not always an ideal measure of similarity between clusters. For example, as shown in Figure 7b, the cluster generated by LDPKiT-Sup visually contains more overlapping data points with the Class 9 cluster compared to LDPKiT-Rand. However, since LDPKiT-Sup incorporates points from both Class 2 and Class 9, its distribution is more dispersed than LDPKiT-Rand which only contains data points from Class 9. Consequently, the centroid of LDPKiT-Rand is slightly closer to the centroid of the Class 9 cluster.

Therefore, to gain a more generalized and comprehensive understanding of the latent space representations, we also evaluate the *Divergence Ratio (DR)* of LDPKiT-Rand’s cluster compared to LDPKiT-Sup’s cluster with respect to the target triplet cluster. To quantify the divergence between clusters, we employ Kullback-Leibler (KL) Divergence [32] defined as follows.

Definition 4.1. KL Divergence. The KL Divergence of two probability distributions P and Q is defined as:

$$D_{\text{KL}}(P||Q) = \sum_x P(x) \log \frac{P(x)}{Q(x)}$$

In our case, we denote the combination of three target clusters as the target triplet cluster, C_T , consisting of all the data points in the triplet classes. The cluster generated by LDPKiT-Sup, denoted as C_S , consists of all superimposed combinations of two target classes, while LDPKiT-Rand’s generated cluster, C_R , consists of noisy data points generated on all three triplet classes. For a fair comparison, C_S and C_R contain the same number of points.

Definition 4.2. Divergence Ratio (DR) between C_S and C_R . The divergence ratio measures how often C_S is less divergent from C_T than C_R to C_T in the context of the KL Divergence.

$$\text{DR}(\bar{C}_R, \bar{C}_S) = \frac{D_{\text{KL}}(\bar{C}_T || \bar{C}_R)}{D_{\text{KL}}(\bar{C}_T || \bar{C}_S)}$$

where \bar{C}_S , \bar{C}_R and \bar{C}_T are normalized distributions that sum to 1. $\text{DR}(\bar{C}_S, \bar{C}_R) > 1$ represents that C_S is less divergent from C_T than C_R within this triplet class setting.

Nuances may occur between different triplets. To evaluate the average-case scenario, we collect statistics across 130 triplets from SVHN, Fashion-MNIST, and PathMNIST and present the results in Table 2. The analysis indicates that LDPKiT-Sup generates clusters that are less divergent from the target triplet cluster, as measured by KL Divergence, in approximately 68.56% of all triplet cases, compared to LDPKiT-Rand. The finding that LDPKiT-Rand tends to diverge from the target distribution more frequently than LDPKiT-Sup match with our previous observations of higher accuracy achieved by LDPKiT-Sup and the insights gained from the latent space analysis. However, it is worth noting that the relationship between accuracy improvement and KL divergence can be complicated.

4.4 RQ3: Sensitivity Analysis on the Impact of $|\mathcal{D}_{\text{infer}}|$ and $|\mathcal{D}_{\text{priv}}|$ on LDPKiT

To study the privacy leakage more thoroughly, we investigate how many private data samples ($|\mathcal{D}_{\text{priv}}|$) are needed for $\mathcal{D}_{\text{infer}}$ construction and how many queries ($|\mathcal{D}_{\text{infer}}|$) are needed to train a \mathcal{M}_L that achieves a reasonable accuracy on $\mathcal{D}_{\text{priv}}$.

As shown in Table 3, we generate several possible $\mathcal{D}_{\text{infer}}$ datasets from $\mathcal{D}_{\text{priv}}$ with varying sizes to examine the effect of $|\mathcal{D}_{\text{priv}}|$ and $|\mathcal{D}_{\text{infer}}|$ on \mathcal{M}_L ’s accuracy. For example, when $\mathcal{D}_{\text{priv}}$ contains 125 points, the largest $\mathcal{D}_{\text{infer}}$ that can be created has 15,500 points (*i.e.*, $|\mathcal{D}_{\text{priv}}| \cdot (|\mathcal{D}_{\text{priv}}| - 1)$). If $|\mathcal{D}_{\text{priv}}|$ is increased to 250, $|\mathcal{D}_{\text{infer}}|$ can still be set to 15,500 by random selection or 62,250 at maximum. For variable control in analyzing LDPKiT’s sensitivity to $|\mathcal{D}_{\text{priv}}|$, an example setting can be fixing $|\mathcal{D}_{\text{infer}}|$ at 15,500 and comparing \mathcal{M}_L ’s accuracies when $|\mathcal{D}_{\text{priv}}|$ is 125 versus when it is 250. Similarly, we can assess the impact of $|\mathcal{D}_{\text{infer}}|$ by fixing $|\mathcal{D}_{\text{priv}}|$ at 250 and comparing the \mathcal{M}_L ’s accuracy for $|\mathcal{D}_{\text{infer}}| = 15,500$ and $|\mathcal{D}_{\text{infer}}| = 62,250$. To identify trends, we exhaustively test some possible pairs of $|\mathcal{D}_{\text{priv}}|$ and $|\mathcal{D}_{\text{infer}}|$ for $|\mathcal{D}_{\text{priv}}|$ ranging from 125 to 1.5k and record ResNet-18 (\mathcal{M}_L)’s accuracies in each scenario.

As shown in Table 3, LDPKiT exhibits low sensitivity to variations in $|\mathcal{D}_{\text{priv}}|$. For instance, the accuracies in the cases with fixed $|\mathcal{D}_{\text{infer}}|$ and varying $|\mathcal{D}_{\text{priv}}|$ are similar across the three benchmarks, *e.g.*, on Fashion-MNIST with $\epsilon = 2.0$, LDPKiT-Sup’s maximum accuracy difference among different $|\mathcal{D}_{\text{priv}}|$ settings is below 5% when $|\mathcal{D}_{\text{infer}}| = 15,500$ and is around 0.69% when $|\mathcal{D}_{\text{infer}}| = 500k$. It also suggests that as long as $|\mathcal{D}_{\text{infer}}|$ is reasonable, the user can generate queries with a smaller $|\mathcal{D}_{\text{priv}}|$, which further reduces privacy risks. There is one case, however ($|\mathcal{D}_{\text{infer}}| = 250k$), where increasing $|\mathcal{D}_{\text{priv}}|$ improves \mathcal{M}_L ’s accuracies. This is likely because a larger training set increases the probability of including more representative and diverse data points that benefit training. However, this improvement is not guaranteed.

Although $|\mathcal{D}_{\text{priv}}|$ is less important, $|\mathcal{D}_{\text{infer}}|$ is capped by its size, and $|\mathcal{D}_{\text{infer}}|$ has more impact on \mathcal{M}_L ’s accuracy. For example, on Path-MNIST with $\epsilon = 10.0$, when $|\mathcal{D}_{\text{priv}}| = 1.5k$, LDPKiT-Rand’s accuracy range from 23.56% with $|\mathcal{D}_{\text{infer}}| = 15,500$ to 54.39% with $|\mathcal{D}_{\text{infer}}| = 500k$. Similarly, LDPKiT-Sup’s accuracy also improved from 42.99% to 76.79% when $|\mathcal{D}_{\text{infer}}|$ increases. The most crucial requirement of $|\mathcal{D}_{\text{infer}}|$ is the sufficient number of data points, *e.g.*, \mathcal{M}_L ’s accuracy is always around 10% for SVHN when $|\mathcal{D}_{\text{infer}}|$ is only 15,500, regardless of $|\mathcal{D}_{\text{priv}}|$.

For a more straightforward visualization of $|\mathcal{D}_{\text{infer}}|$ ’s impact, we also present \mathcal{M}_L ’s accuracies with the setting of $|\mathcal{D}_{\text{priv}}| = 1.5k$ with varying $|\mathcal{D}_{\text{infer}}|$ as bar graphs in Figure 8. Notably, a reasonably large $\mathcal{D}_{\text{infer}}$ is required for LDPKiT-Sup to have an adequate accuracy (*e.g.*, 250k for PathMNIST and 500k for Fashion-MNIST and SVHN). While increasing $|\mathcal{D}_{\text{infer}}|$ enhances accuracy, the improvement becomes marginal once $|\mathcal{D}_{\text{infer}}|$ exceeds 500k. For instance, ResNet-18 (\mathcal{M}_L) reaches 74.35%, 78.88% and 81.78% accuracies on $\mathcal{D}_{\text{priv}}$ of Fashion-MNIST when it is trained on $\mathcal{D}_{\text{infer}}$ with ϵ set to 2.0 and sizes of 500k, 1M and 2.2M, respectively. In other words, it is unnecessary to query all possible data points in $\mathcal{D}_{\text{cand}}$, as discussed in Section 4.2. The trained \mathcal{M}_L with LDPKiT-Sup can achieve satisfactory accuracies using only

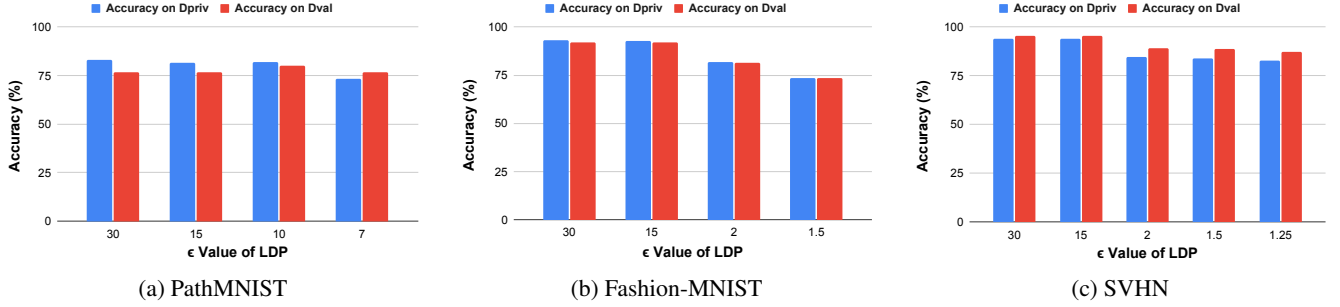


Figure 9: Impact of ϵ values on ResNet-18 (\mathcal{M}_L)’s accuracies on $\mathcal{D}_{\text{priv}}$ versus \mathcal{D}_{val} with LDPKiT-Sup.

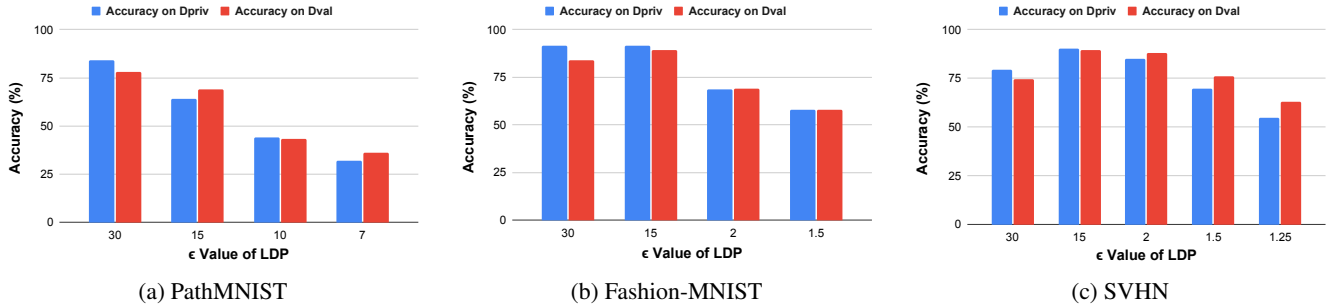


Figure 10: Impact of ϵ values on ResNet-18 (\mathcal{M}_L)’s accuracies on $\mathcal{D}_{\text{priv}}$ versus \mathcal{D}_{val} with LDPKiT-Rand.

about 20% of $\mathcal{D}_{\text{infer}}$ for querying. Appendix D.3 presents the evaluation results for other ϵ values on the same benchmarks. The results match the conclusions drawn from Figure 8.

It is important to note that the subsets of $\mathcal{D}_{\text{infer}}$ used to train \mathcal{M}_L are randomly selected in this section of experiments. More advanced methods, such as active learning and core-set strategies [26, 33], could be employed to identify a smaller yet representative subset of $\mathcal{D}_{\text{infer}}$, effectively approximating the full dataset’s ability to train the model or capture the dataset’s overall distribution. Exploring such data selection methods for $\mathcal{D}_{\text{infer}}$ size reduction is left for future work.

4.5 Effect of Noise on Overfitting to $\mathcal{D}_{\text{priv}}$ and Generalization to \mathcal{D}_{val} Across ϵ Values

LDP bounds privacy leakage rather than eliminating it. As defined in Definition 2.1, larger ϵ values reduce the LDP noise, weakening privacy protections. In reality, the user is interested in labelling $\mathcal{D}_{\text{priv}}$. However, to safeguard privacy, she may choose to query only a subset of $\mathcal{D}_{\text{priv}}$ while maintaining a reasonable $|\mathcal{D}_{\text{infer}}|$ and label the rest of the data she never queried with the extracted \mathcal{M}_L model if it can generalize to unseen data points \mathcal{D}_{val} (*i.e.*, also attributes to $|\mathcal{D}_{\text{priv}}|$ insensitivity as discussed in Section D.3). To explore this, we analyze the impact of ϵ on generalization. Improved generalization implies better privacy, as the user can reduce $|\mathcal{D}_{\text{priv}}|$ for generating queries while still extracting a model that generalizes to the remaining private data. Figures 9 and 10 show that

ResNet-18 (\mathcal{M}_L) achieves higher accuracy on $\mathcal{D}_{\text{priv}}$ than on \mathcal{D}_{val} when ϵ is high (weaker privacy protection), particularly with LDPKiT-Rand. As ϵ decreases, \mathcal{D}_{val} accuracy improves, eventually matching or exceeding $\mathcal{D}_{\text{priv}}$ accuracy, indicating reduced overfitting and better generalization. Similar trends are observed with MobileNetV2 in Figures 14 and 15 in Appendix D.2. Therefore, the user may obtain better privacy protection by reducing $|\mathcal{D}_{\text{priv}}|$ while she increases ϵ . Further analysis can be performed to provide deeper insights. For instance, we can measure privacy leakage using metrics such as membership inference attack success rates and attribute inference metrics to help examine the relationship between ϵ , overfitting and privacy leakage. We can also analyze the mutual information between $\mathcal{D}_{\text{priv}}$ and $\mathcal{D}_{\text{infer}}$ under different ϵ settings. We leave the analyses as future work.

5 Related work

Knowledge transfer techniques. Knowledge distillation is a knowledge transfer technique that distills a large teacher model into a smaller student model while preserving model performance [34–40]. The conventional use case is model compression, enabling the model deployment in a resource-restricted environment. Knowledge can be transferred in different forms, such as logits, model parameters, intermediate layers’ activations or features, and their interrelationships [35]. Knowledge transfer also has adversarial applica-

tions. A model extraction attack is an adversarial example in which the attacker reproduces a model stealthily by stealing its parameters, decision boundaries, or functionalities. It demonstrates that an iterative query-based knowledge transfer process from a high-performance model can be performed via a prediction query interface [41–43]. Model extraction can be challenging without knowledge of the victim model’s training data distribution [44], successful model extractions with partial or zero knowledge of the victim model and training data [42, 44–47] can be costly in queries and require more information than hard labels. Related defences [48–51] and analyses [52, 53] are also in active research. Rather than model compression or extraction, we incorporate knowledge transfer for privacy preservation in a non-adversarial manner to recover the utility loss brought by LDP. Therefore, regarding the accuracies, our mechanism still demonstrates the privacy-utility trade-off rather than creating a competitive surrogate model that violates cloud services’ terms of use. We qualitatively and quantitatively demonstrate that LDPKiT differs from the model extraction attack in Section 6.1.

Noise injection and differential privacy (DP). DP can be used either locally [54] or globally [55–57], and both methods provide provable privacy guarantees. Global differential privacy (GDP) shares original input data with a trusted data curator, which then applies noise to the aggregated data. In this case, the curator has access to the original sensitive data. To remove this point of trust, LDPKiT uses a local differential privacy (LDP) mechanism. In LDP, the data source (*i.e.*, the user) adds noise to each individual query before data transmission to the cloud, so she has full control over privacy protection. The side effect is that the noise is aggregated on the cloud, so LDP methods usually provide lower utility than GDP at the same level of privacy protection (*i.e.*, noise level). While we add noise to original inputs before offloading inference to the cloud, similar to [15], noise can also be injected into inference frameworks deployed on a split computation setting [58–61], where the DNN is partitioned between the cloud and edge devices. These schemes involve a white-box model, so noise can be added to intermediate representations, which is different from our setting. A common challenge of DP schemes is to find a balance between utility and privacy.

Other privacy protection techniques. One class of privacy protection methods is data encryption with homomorphic algorithms, which suffers from high computational overheads [12, 13]. In contrast, LDPKiT is more efficient, as it does not require complicated computation to be performed for each query. Hardware-assisted inference in Trusted Execution Environments (TEEs) is another approach [14]. A TEE is a secure area within a processor that provides a safe environment for sensitive code execution, preventing unauthorized access. Slalom puts the computation in a TEE to address inference privacy on remote services [14]. However, Slalom does

not protect against the risks of side-channel attacks. Since TEEs have access to the original data, privacy breaches can still happen if the attackers compromise the TEEs [62–64]. Side-channels are not a threat for LDPKiT since it does not transmit the original data, and any privacy leakage is bounded by the LDP noise.

6 Discussion and Limitations

6.1 Ethical Use of Model Extraction Principles

While our approach involves knowledge transfer from a remote model to a local model, it differs from adversarial model extraction attacks [42, 44–47]. The deployment of LDPKiT does not aim to replicate the economic value of commercial models or compete with model owners. Instead, LDPKiT ethically integrates model extraction principles to protect user inference data information, prioritizing data privacy over adversarial exploitation.

Existing defenses against model extraction attacks often lack generalizability [19, 21], and advanced techniques [20] can bypass them, risking economic losses for commercial model owners. However, this is not a concern in our case. LDPKiT’s extraction objective focuses solely on protecting data privacy, not economic gain. At fairly privacy-protective noise levels, such as when SIDP drops to approximately 25%, the \mathcal{M}_L model generated by LDPKiT exhibits an accuracy trade-off for privacy ranging from 10% to 30%, depending on the noise level, model and dataset. Notably, \mathcal{M}_L is not competitive with \mathcal{M}_R ; for instance, ResNet-18 (\mathcal{M}_L) show accuracy drops of 12.96% and 21.23% on Fashion-MNIST with LDPKiT-Sup at ϵ values of 2.0 and 1.5, respectively. Given this lack of competitiveness, \mathcal{M}_L does not serve the objectives of adversarial model extraction and adheres to the non-competition terms of use outlined by major commercial model providers [18].

Furthermore, we assess the similarity between \mathcal{M}_L created by LDPKiT and \mathcal{M}_R in Section 4.2 using *Zest* distances [65]. *Zest* is a detection scheme for model extraction attacks that computes distances between two models based on LIME’s model-agnostic explanations [66]. We use *Zest* because of its architecture independence, the model’s black-box access requirement, and its perfect accuracy in model extraction detection with *Cosine* distance metric. *Zest* supports l_1 , l_2 , l_∞ norm and *Cosine* distances. According to the authors of *Zest*, the method achieves 100% accuracy in detecting model extraction attacks when employing the *Cosine* distance metric [65], which is the metric presented in Table 4. Details of the detection procedure are outlined in Appendix E.1. We present the normalized *Zest* distances, \overline{D}_z , with the *Cosine* distance metric in Table 4. Results for other supported metrics are provided in Appendix E.2. As explained in Appendix E.1, an adversarial model extraction attack occurs when $\overline{D}_z < 1$. Table 4 shows that LDPKiT does not contribute to model theft

Table 4: Normalized Zest distance results with *Cosine* distance metric on \mathcal{M}_R and \mathcal{M}_L .

\mathcal{M}_R	\mathcal{M}_L	Mechanism	Fashion-MNIST		SVHN		PathMNIST	
			$\epsilon=2.0$	$\epsilon=1.5$	$\epsilon=1.5$	$\epsilon=1.25$	$\epsilon=10.0$	$\epsilon=7.0$
ResNet-152	ResNet-18	LDPKiT-Sup	2.5598	3.2729	1.1948	1.1859	5.3133	5.4322
		LDPKiT-Rand	3.6643	4.2645	1.6503	2.4100	6.1018	4.2305
	MobileNetV2	LDPKiT-Sup	5.5795	5.1662	1.3259	1.2905	7.2874	7.2874
		LDPKiT-Rand	3.1595	2.7800	1.6183	1.7758	7.2874	7.2874

An adversarial model extraction attack is detected if the normalized Zest distance is smaller than 1.0.

at any noise level since all $\overline{D}_z > 1$. In conclusion, the Zest results confirm that the extracted \mathcal{M}_L model does not closely mimic \mathcal{M}_R and primarily serves to recover utility for \mathcal{D}_{priv} . Combined with Section 4 results, these findings validate the ethical application of model extraction principles in LDPKiT, while upholding privacy objectives without compromising the benefits, rights or interests of any stakeholders.

6.2 Limitations and Future Work

For the limitations, as discussed in Section 3, the per-query ϵ -LDP privacy guarantee only holds under the assumption that each data point in \mathcal{D}_{priv} is *i.i.d.*. If they are not *i.i.d.*, our privacy guarantee will be weakened by their mutual information. Many real-world applications may use data de-duplication technologies to maintain the *i.i.d.* assumption for data management, ensuring data integrity and preventing redundancy. For instance, cloud storage services such as Amazon S3 identify and delete duplicated objects to optimize user’s storage space [67]. Entities and businesses such as credit bureaus and e-commerce platforms use de-duplication techniques to merge and resolve records based on attributes (*e.g.*, names, birth dates, and addresses), even when minor differences exist.

As discussed in Section 4.4, LDPKiT is compatible with advanced training strategies, such as active learning, that expedite model training and help training set size reduction. Active learning strategies can also be applied to prune queries in \mathcal{D}_{infer} that are less significant. We plan to study the effect of such strategies on LDPKiT in the future. Furthermore, since \mathcal{M}_L is trained on noisy data, LDPKiT is inherently immune to membership inference attacks if \mathcal{M}_L is ever leaked. We leave the analyses of membership inference and attribute inference attack success rates as future work.

Due to time constraints, we only tested on supervised learning, specifically classification tasks. In the future, we may extend the evaluation to regression tasks or unsupervised clustering tasks. Furthermore, while the empirical analyses in Section 4 focus on image benchmarks, extending LDPKiT to other modalities, such as text, is part of our future work.

Also, our privacy-preserving queries in this paper refer to LDPKiT-generated noised queries with LDPKiT-Rand or

LDPKiT-Sup utilizing ϵ -LDP privacy mechanism. We can generate such queries in other ways. For instance, LDPKiT is compatible with other noise mechanisms such as (ϵ, δ) -LDP with the Gaussian mechanism. In addition, we can also compose our privacy-preserving \mathcal{D}_{priv} by generating synthetic queries using a Generative Adversarial Network [68].

7 Conclusion

LDPKiT is an inference framework designed to protect the privacy of sensitive data when using privacy-sensitive yet potentially malicious cloud services. LDPKiT achieves privacy protection by introducing LDP noise into the data before transmission to the cloud model for inference, ensuring privacy even if the platform or model is compromised. Moreover, LDPKiT mitigates the accuracy loss with a two-layer noise injection mechanism, *e.g.*, LDPKiT-Rand and LDPKiT-Sup, leveraging the post-processing property of LDP. The base noise ensures privacy protection, while the second layer of noise helps utility recovery by generating sufficient data points that closely approximate the target distribution of the private data for local training. The key insight is that effective yet privacy-preserving knowledge transfer requires the user to query a sufficient amount of privacy-protected noised data points that have a closer distribution to the actual private data. Superimposition in LDPKiT-Sup creates such a dataset that is more representative than LDPKiT-Rand which adds unrelated noise. The experimental results show that LDPKiT-Sup successfully recovers prediction accuracy on private data during training while preserving privacy. Furthermore, quantitative analysis such as latent space analysis confirms the accuracy improvements. LDPKiT-Sup has greater benefits with higher noise levels, corresponding to stronger privacy guarantees. LDPKiT employs knowledge transfer and model extraction techniques while adhering to cloud service’s terms of use by limiting use to non-commercial purposes and ensuring derived models do not compete commercially. Additionally, quantitative evaluations confirm that the knowledge transfer in LDPKiT does not facilitate adversarial model extraction attacks, reinforcing its ethical and secure design.

8 Ethics Consideration

The author(s) attest that they read and follow the USENIX Security '25 Ethics Guidelines. This research is conducted with a strong commitment to ethical integrity. This discussion of ethics consideration focuses on identifying stakeholders, assessing potential risks, implementing mitigations, and justifying key decisions. The primary stakeholders include service providers offering the cloud service platform, end users whose private data may be transmitted to the cloud and face potential privacy risks, and research team member(s). Given the use of knowledge transfer and model extraction techniques in this research, the experiments could potentially conflict with the Terms of Service set by the service providers. However, the authors affirm that the extraction techniques employed do not violate these Terms of Service and do not constitute an adversarial model extraction attack (*i.e.*, model theft). Further details are provided in Section 6.1 of the paper.

Additionally, the authors confirm that the research does not compromise end users' private data. Instead, it focuses on developing a privacy-preserving framework that safeguards user data privacy in the context of cloud ML applications.

Lastly, the research activities have been conducted with care to ensure there is no negative impact on the wellbeing of research team member(s).

9 Open science

The author(s) attest that they comply with the USENIX Security '25 Open Science Policies. The author(s) will make the research artifacts available to the public upon paper acceptance. Specifically, the source code and scripts will be shared to ensure the availability, functionality and reproducibility of the research artifacts, facilitating further research and development in this area.

References

- [1] C. Savage and N. Perlroth, "Yahoo said to have aided U.S. email surveillance by adapting spam filter," Oct 2016. [Online]. Available: <https://www.nytimes.com/2016/10/06/technology/yahoo-email-tech-companies-government-investigations.html>
- [2] P. Dave and B. Bennet, "Yahoo helped the U.S. Government spy on emails, report says," Oct 2016. [Online]. Available: <https://www.latimes.com/business/technology/la-fi-tn-yahoo-email-20161004-snap-story.html>
- [3] D. Kaye, "Reports that Yahoo aided us e-mail surveillance draw concern of UN Human Rights Expert | UN News," Oct 2016. [Online]. Available: <https://news.un.org/en/story/2016/10/542152>
- [4] A. NG, "Amazon gave ring videos to police without owners' permission," Jul 2022. [Online]. Available: <https://www.politico.com/news/2022/07/13/amazon-gave-ring-videos-to-police-without-owners-permission-00045513>
- [5] S. Ray, "Apple joins a growing list of companies cracking down on use of chatgpt by staffers—here's why," Oct 2023. [Online]. Available: <https://www.forbes.com/sites/siladityaray/2023/05/19/apple-joins-a-growing-list-of-companies-cracking-down-on-use-of-chatgpt-by-staffers-heres-why/>
- [6] N. Gordon, "Apple restricts employee chatgpt use as companies worry about data leaks," May 2023. [Online]. Available: <https://fortune.com/2023/05/19/apple-restricts-chatgpt-employee-data-leaks-iphone/>
- [7] Y. Xu, W. Cui, and M. Peinado, "Controlled-channel attacks: Deterministic side channels for untrusted operating systems," in *IEEE Symposium on Security and Privacy*, 2015.
- [8] A. Esteva, B. Kuprel, R. A. Novoa, J. Ko, S. M. Swetter, H. M. Blau, and S. Thrun, "Dermatologist-level classification of skin cancer with deep neural networks," *nature*, vol. 542, no. 7639, pp. 115–118, 2017.
- [9] A. Esteva, A. Robicquet, B. Ramsundar, V. Kuleshov, M. DePristo, K. Chou, C. Cui, G. Corrado, S. Thrun, and J. Dean, "A guide to deep learning in healthcare," *Nature medicine*, vol. 25, no. 1, pp. 24–29, 2019.
- [10] W. Hilal, S. A. Gadsden, and J. Yawney, "Financial fraud: a review of anomaly detection techniques and recent advances," *Expert systems With applications*, vol. 193, p. 116429, 2022.
- [11] M. Taib, J. Wu, S. Drew, and G. G. Messier, "Enhancing equitable access to ai in housing and homelessness system of care through federated learning," in *Proceedings of the AAAI/ACM Conference on AI, Ethics, and Society*, vol. 7, 2024, pp. 1434–1443.
- [12] N. Dowlin, R. Gilad-Bachrach, K. Laine, K. Lauter, M. Naehrig, and J. Wernsing, "CryptoNets: Applying Neural Networks to Encrypted Data with High Throughput and Accuracy," Tech. Rep. MSR-TR-2016-3, February 2016. [Online]. Available: <https://www.microsoft.com/en-us/research/publication/cryptonets-applying-neural-networks-to-encrypted-data-with-high-throughput-and-accuracy>
- [13] C. Juvekar, V. Vaikuntanathan, and A. Chandrakasan, "Gazelle: A Low Latency Framework for Secure Neural Network Inference," 2018. [Online]. Available: <https://arxiv.org/abs/1801.05507>

- [14] F. Tramèr and D. Boneh, “Slalom: Fast, Verifiable and Private Execution of Neural Networks in Trusted Hardware,” 2019.
- [15] S. Leroux, T. Verbelen, P. Simoens, and B. Dhoedt, “Privacy Aware Offloading of Deep Neural Networks,” 2018.
- [16] M. Li, Y. Tian, J. Zhang, D. Fan, and D. Zhao, “The trade-off between privacy and utility in local differential privacy,” in *2021 International Conference on Networking and Network Applications (NaNA)*, 2021, pp. 373–378.
- [17] Z. Tzermias, V. Prevelakis, and S. Ioannidis, “Privacy risks from public data sources,” in *ICT Systems Security and Privacy Protection: 29th IFIP TC 11 International Conference, SEC 2014, Marrakech, Morocco, June 2-4, 2014. Proceedings 29*. Springer, 2014, pp. 156–168.
- [18] OpenAI, “Terms of use,” <https://openai.com/policies/terms-of-use/>.
- [19] H. Yao, Z. Li, H. Weng, F. Xue, Z. Qin, and K. Ren, “Fdinet: Protecting against dnn model extraction via feature distortion index,” 2024. [Online]. Available: <https://arxiv.org/abs/2306.11338>
- [20] Y. Chen, R. Guan, X. Gong, J. Dong, and M. Xue, “Ddae: Defense-penetrating model extraction attacks,” in *2023 IEEE Symposium on Security and Privacy (SP)*, 2023, pp. 382–399.
- [21] M. Juuti, S. Szyller, S. Marchal, and N. Asokan, “Prada: Protecting against dnn model stealing attacks,” in *2019 IEEE European Symposium on Security and Privacy (EuroS&P)*, 2019, pp. 512–527.
- [22] C. Dwork, F. McSherry, K. Nissim, and A. Smith, “Calibrating noise to sensitivity in private data analysis,” in *Theory of Cryptography: Third Theory of Cryptography Conference, TCC 2006, New York, NY, USA, March 4-7, 2006. Proceedings 3*. Springer, 2006, pp. 265–284.
- [23] C. Dwork and A. Roth, “The Algorithmic Foundations of Differential Privacy,” *Found. Trends Theor. Comput. Sci.*, vol. 9, no. 3–4, p. 211–407, aug 2014. [Online]. Available: <https://doi.org/10.1561/04000000042>
- [24] Z. Wang and J. P. Reiter, “Post-processing differentially private counts to satisfy additive constraints,” *Trans. Data Priv.*, vol. 14, pp. 65–77, 2021. [Online]. Available: <https://api.semanticscholar.org/CorpusID:237521561>
- [25] B. Settles, “Active learning literature survey,” 2009.
- [26] O. Sener and S. Savarese, “Active learning for convolutional neural networks: A core-set approach,” *arXiv preprint arXiv:1708.00489*, 2017.
- [27] Y. Netzer, T. Wang, A. Coates, A. Bissacco, B. Wu, and A. Y. Ng, “Reading digits in natural images with unsupervised feature learning,” 2011.
- [28] H. Xiao, K. Rasul, and R. Vollgraf, “Fashion-mnist: a novel image dataset for benchmarking machine learning algorithms,” *arXiv preprint arXiv:1708.07747*, 2017.
- [29] J. Yang, R. Shi, D. Wei, Z. Liu, L. Zhao, B. Ke, H. Pfister, and B. Ni, “Medmnist v2-a large-scale lightweight benchmark for 2d and 3d biomedical image classification,” *Scientific Data*, vol. 10, no. 1, p. 41, 2023.
- [30] K. He, X. Zhang, S. Ren, and J. Sun, “Deep Residual Learning for Image Recognition,” 2015.
- [31] M. Sandler, A. Howard, M. Zhu, A. Zhmoginov, and L.-C. Chen, “MobileNetV2: Inverted Residuals and Linear Bottlenecks,” 2019.
- [32] S. Kullback and R. A. Leibler, “On information and sufficiency,” *The Annals of Mathematical Statistics*, vol. 22, no. 1, pp. 79–86, 1951.
- [33] B. Settles, “From theories to queries: Active learning in practice,” in *Active Learning and Experimental Design workshop In conjunction with AISTATS 2010*, ser. Proceedings of Machine Learning Research, I. Guyon, G. Cawley, G. Dror, V. Lemaire, and A. Statnikov, Eds., vol. 16. Sardinia, Italy: PMLR, 16 May 2011, pp. 1–18. [Online]. Available: <https://proceedings.mlr.press/v16/settles11a.html>
- [34] G. Hinton, O. Vinyals, and J. Dean, “Distilling the knowledge in a neural network,” *arXiv preprint arXiv:1503.02531*, 2015.
- [35] J. Gou, B. Yu, S. J. Maybank, and D. Tao, “Knowledge Distillation: A Survey,” *Int. J. Comput. Vision*, vol. 129, no. 6, p. 1789–1819, jun 2021. [Online]. Available: <https://doi.org/10.1007/s11263-021-01453-z>
- [36] A. Romero, N. Ballas, S. E. Kahou, A. Chassang, C. Gatta, and Y. Bengio, “FitNets: Hints for Thin Deep Nets,” 2015.
- [37] K. Xu, L. Rui, Y. Li, and L. Gu, “Feature normalized knowledge distillation for image classification,” in *Computer Vision—ECCV 2020: 16th European Conference, Glasgow, UK, August 23–28, 2020, Proceedings, Part XXV 16*. Springer, 2020, pp. 664–680.
- [38] S. Zagoruyko and N. Komodakis, “Paying more attention to attention: Improving the performance of convolutional neural networks via attention transfer,” *arXiv preprint arXiv:1612.03928*, 2016.

- [39] F. Tung and G. Mori, "Similarity-preserving knowledge distillation," in *Proceedings of the IEEE/CVF International Conference on Computer Vision*, 2019, pp. 1365–1374.
- [40] W. Park, D. Kim, Y. Lu, and M. Cho, "Relational Knowledge Distillation," in *Proceedings of the IEEE/CVF Conference on Computer Vision and Pattern Recognition (CVPR)*, June 2019.
- [41] F. Tramèr, F. Zhang, A. Juels, M. K. Reiter, and T. Ristenpart, "Stealing Machine Learning Models via Prediction APIs." in *USENIX security symposium*, vol. 16, 2016, pp. 601–618.
- [42] J. Zhang, C. Chen, and L. Lyu, "IDEAL: Query-Efficient Data-Free Learning from Black-Box Models," in *The Eleventh International Conference on Learning Representations*, 2022.
- [43] S. Lee, G. Lee, J. W. Kim, J. Shin, and M.-K. Lee, "HETAL: Efficient privacy-preserving transfer learning with homomorphic encryption," in *Proceedings of the 40th International Conference on Machine Learning*, ser. Proceedings of Machine Learning Research, A. Krause, E. Brunskill, K. Cho, B. Engelhardt, S. Sabato, and J. Scarlett, Eds., vol. 202. PMLR, 23–29 Jul 2023, pp. 19 010–19 035. [Online]. Available: <https://proceedings.mlr.press/v202/lee23m.html>
- [44] J.-B. Truong, P. Maini, R. J. Walls, and N. Papernot, "Data-free model extraction," in *Proceedings of the IEEE/CVF conference on computer vision and pattern recognition*, 2021, pp. 4771–4780.
- [45] N. Papernot, P. McDaniel, I. Goodfellow, S. Jha, Z. B. Celik, and A. Swami, "Practical Black-Box Attacks against Machine Learning," in *Proceedings of the 2017 ACM on Asia Conference on Computer and Communications Security*, ser. ASIA CCS '17. New York, NY, USA: Association for Computing Machinery, 2017, p. 506–519. [Online]. Available: <https://doi.org/10.1145/3052973.3053009>
- [46] S. Pal, Y. Gupta, A. Shukla, A. Kanade, S. K. Shevade, and V. Ganapathy, "Activethief: Model extraction using active learning and unannotated public data," in *The Thirty-Fourth AAAI Conference on Artificial Intelligence, AAAI 2020, The Thirty-Second Innovative Applications of Artificial Intelligence Conference, IAAI 2020, The Tenth AAAI Symposium on Educational Advances in Artificial Intelligence, EAAI 2020, New York, NY, USA, February 7-12, 2020*. AAAI Press, 2020, pp. 865–872. [Online]. Available: <https://doi.org/10.1609/aaai.v34i01.5432>
- [47] T. Orekondy, B. Schiele, and M. Fritz, "Knockoff Nets: Stealing Functionality of Black-Box Models," 2018.
- [48] H. Chen, B. D. Rouhani, C. Fu, J. Zhao, and F. Koushanfar, "DeepMarks: A Secure Fingerprinting Framework for Digital Rights Management of Deep Learning Models," in *Proceedings of the 2019 on International Conference on Multimedia Retrieval*, ser. ICMR '19. New York, NY, USA: Association for Computing Machinery, 2019, p. 105–113. [Online]. Available: <https://doi.org/10.1145/3323873.3325042>
- [49] Y. Adi, C. Baum, M. Cisse, B. Pinkas, and J. Keshet, "Turning Your Weakness Into a Strength: Watermarking Deep Neural Networks by Backdooring," 2018.
- [50] A. Dziedzic, M. A. Kaleem, Y. S. Lu, and N. Papernot, "Increasing the Cost of Model Extraction with Calibrated Proof of Work," 2022.
- [51] Y. Liu, K. Li, Z. Liu, B. Wen, K. Xu, W. Wang, W. Zhao, and Q. Li, "Provenance of Training without Training Data: Towards Privacy-Preserving DNN Model Ownership Verification," in *Proceedings of the ACM Web Conference 2023*, ser. WWW '23. New York, NY, USA: Association for Computing Machinery, 2023, p. 1980–1990. [Online]. Available: <https://doi.org/10.1145/3543507.3583198>
- [52] A. Dziedzic, N. Dhawan, M. A. Kaleem, J. Guan, and N. Papernot, "On the Difficulty of Defending Self-Supervised Learning against Model Extraction," 2022.
- [53] V. Chandrasekaran, K. Chaudhuri, I. Giacomelli, S. Jha, and S. Yan, "Exploring Connections between Active Learning and Model Extraction," in *Proceedings of the 29th USENIX Conference on Security Symposium*, ser. SEC'20. USA: USENIX Association, 2020.
- [54] U. Erlingsson, V. Pihur, and A. Korolova, "RAPPOR: Randomized Aggregatable Privacy-Preserving Ordinal Response," in *Proceedings of the 2014 ACM SIGSAC Conference on Computer and Communications Security*, ser. CCS '14. New York, NY, USA: Association for Computing Machinery, 2014, p. 1054–1067. [Online]. Available: <https://doi.org/10.1145/2660267.2660348>
- [55] N. Papernot, S. Song, I. Mironov, A. Raghunathan, K. Talwar, and Úlfar Erlingsson, "Scalable Private Learning with PATE," 2018.
- [56] M. Abadi, A. Chu, I. Goodfellow, H. B. McMahan, I. Mironov, K. Talwar, and L. Zhang, "Deep Learning with Differential Privacy," in *Proceedings of the 2016 ACM SIGSAC Conference on Computer and Communications Security*. ACM, oct 2016. [Online]. Available: <https://doi.org/10.1145%2F2976749.2978318>

- [57] Y. Zhu, X. Yu, M. Chandraker, and Y.-X. Wang, "Private-kNN: Practical Differential Privacy for Computer Vision," in *2020 IEEE/CVF Conference on Computer Vision and Pattern Recognition (CVPR)*, 2020, pp. 11 851–11 859.
- [58] L. Lyu, J. C. Bezdek, J. Jin, and Y. Yang, "FORESEEN: Towards Differentially Private Deep Inference for Intelligent Internet of Things," *IEEE Journal on Selected Areas in Communications*, vol. 38, no. 10, pp. 2418–2429, 2020.
- [59] F. Mireshghallah, M. Taram, P. Ramrakhani, A. Jalali, D. Tullsen, and H. Esmailzadeh, "Shredder: Learning noise distributions to protect inference privacy," in *Proceedings of the Twenty-Fifth International Conference on Architectural Support for Programming Languages and Operating Systems*, 2020, pp. 3–18.
- [60] S. A. Osia, A. Shahin Shamsabadi, S. Sajadmanesh, A. Taheri, K. Katevas, H. R. Rabiee, N. D. Lane, and H. Haddadi, "A Hybrid Deep Learning Architecture for Privacy-Preserving Mobile Analytics," *IEEE Internet of Things Journal*, vol. 7, no. 5, pp. 4505–4518, 2020.
- [61] J. Wang, J. Zhang, W. Bao, X. Zhu, B. Cao, and P. S. Yu, "Not Just Privacy: Improving Performance of Private Deep Learning in Mobile Cloud," 2018. [Online]. Available: <https://arxiv.org/abs/1809.03428>
- [62] J. Van Bulck, M. Minkin, O. Weisse, D. Genkin, B. Kasikci, F. Piessens, M. Silberstein, T. F. Wensch, Y. Yarom, and R. Strackx, "Foreshadow: Extracting the keys to the Intel SGX kingdom with transient Out-of-Order execution," in *27th USENIX Security Symposium (USENIX Security 18)*, 2018, pp. 991–1008.
- [63] M. Schwarz, M. Lipp, D. Moghimi, J. Van Bulck, J. Stecklina, T. Prescher, and D. Gruss, "ZombieLoad: Cross-privilege-boundary data sampling," in *Proceedings of the 2019 ACM SIGSAC Conference on Computer and Communications Security*, 2019, pp. 753–768.
- [64] M. Lipp, M. Schwarz, D. Gruss, T. Prescher, W. Haas, J. Horn, S. Mangard, P. Kocher, D. Genkin, Y. Yarom *et al.*, "Meltdown: Reading kernel memory from user space," *Communications of the ACM*, vol. 63, no. 6, pp. 46–56, 2020.
- [65] H. Jia, H. Chen, J. Guan, A. S. Shamsabadi, and N. Papernot, "A Zest of LIME: Towards Architecture-Independent Model Distances," in *International Conference on Learning Representations*, 2021.
- [66] M. T. Ribeiro, S. Singh, and C. Guestrin, "'Why should I trust you?' Explaining the predictions of any classifier," in *Proceedings of the 22nd ACM SIGKDD international conference on knowledge discovery and data mining*, 2016, pp. 1135–1144.
- [67] T. Lim, "Managing duplicate objects in amazon s3," Jan 2024. [Online]. Available: <https://aws.amazon.com/blogs/storage/managing-duplicate-objects-in-amazon-s3/>
- [68] I. J. Goodfellow, J. Pouget-Abadie, M. Mirza, B. Xu, D. Warde-Farley, S. Ozair, A. Courville, and Y. Bengio, "Generative adversarial networks," 2014. [Online]. Available: <https://arxiv.org/abs/1406.2661>

A Proof of ϵ -LDP with the Laplacian mechanism and Post-Processing Property

We discuss the proof aforementioned in Section 3 here: We prove that the base noise injection scheme (i.e., the first layer of noise) that generates $\mathcal{D}_{\text{protected}}$ satisfies the definition of ϵ -LDP with the Laplacian mechanism in Theorem A.1.

Theorem A.1. *Our base noise injection mechanism satisfies ϵ -LDP where $\epsilon = \frac{\Delta_f}{\lambda}$*

Proof. Let v be the original data and $f(v)$ be the query and computation function performed on the data with function sensitivity, $\Delta_f = \max_{v_1, v_2} \|f(v_2) - f(v_1)\|_1$. We define the randomization algorithm \mathcal{A} with Laplacian mechanism such that for any input value v , $\mathcal{A} = f(v) + \mathcal{Z}$, where \mathcal{Z} is sampled from the Laplacian distribution $L(z, \lambda)$ with scaling factor λ set to $\frac{\Delta_f}{\epsilon}$.

The probability that \mathcal{A} has an output $s \in \mathcal{S}$ given an input v can be expressed as:

$$\begin{aligned} \Pr[\mathcal{A}(v) = s] &= \Pr[f(v) + \mathcal{Z} = s] \\ &= \Pr[\mathcal{Z} = s - f(v)] \\ &= \frac{1}{2\lambda} \exp\left(-\frac{|s - f(v)|}{\lambda}\right) \end{aligned}$$

for all $s \in \mathcal{S}$.

To satisfy ϵ -LDP, we need Equation 1 to hold for any output $s \in \mathcal{S}$ and any input pairs v_1 and v_2 .

By substituting the PDF of Laplacian distribution's new expression into the Equation 1, we get

$$\frac{1}{2\lambda} \exp\left(-\frac{|s - f(v_1)|}{\lambda}\right) \leq e^\epsilon \frac{1}{2\lambda} \exp\left(-\frac{|s - f(v_2)|}{\lambda}\right)$$

which simplifies to

$$\exp\left(\frac{|s - f(v_2)| - |s - f(v_1)|}{\lambda}\right) \leq e^\epsilon$$

With $\lambda = \frac{\Delta_f}{\epsilon}$, the equation becomes:

$$\exp\left(\epsilon \cdot \frac{|s - f(v_1)| - |s - f(v_2)|}{\Delta_f}\right) \leq e^\epsilon \quad (4)$$

for all pairs of v_1 and v_2 .

Since $|s - f(v_1)| - |s - f(v_2)| \leq \Delta_f$ by the definition of sensitivity function, Equation 4 always holds. \square

Then, we prove that our noise generation algorithms, LDPKiT-Rand and LDPKiT-Sup, satisfy the post-processing property of LDP and hence provide the same level of ϵ -LDP privacy guarantee on $\mathcal{D}_{\text{infer}}$ as $\mathcal{D}_{\text{protected}}$.

Theorem A.2. *Our noise injection mechanism LDPKiT-Rand satisfies ϵ -LDP.*

Proof. For each data point $d_i \in \mathcal{D}_{\text{priv}}$, where $i = 1, 2, \dots, |\mathcal{D}_{\text{priv}}|$, apply the Laplacian mechanism (See Definition 2.2) to obtain the first noise-added data point:

$$\tilde{d}_i^{(1)} = d_i + \eta_i^{(1)},$$

where $\eta_i^{(1)}$ is a random variable drawn from the Laplacian distribution with scaling factor $\lambda = \frac{\Delta_f}{\epsilon}$.

By Definition 2.1, this initial mechanism satisfies ϵ -LDP.

As for the post-processing step in LDPKiT-Rand, for each $\tilde{d}_i^{(1)}$, we generate $|\mathcal{D}_{\text{priv}}| - 1$ distinct random versions by adding an additional layer of Laplacian noise with the same scale:

$$\tilde{d}_{i,j}^{(2)} = \tilde{d}_i^{(1)} + \eta_{i,j}^{(2)}, \quad \text{for } j = 1, 2, \dots, |\mathcal{D}_{\text{priv}}| - 1,$$

where $\eta_{i,j}^{(2)}$ are independent random variables drawn from the Laplacian distribution with scaling factor $\lambda = \frac{\Delta_f}{\epsilon}$.

This step is considered post-processing because it operates on $\tilde{d}_i^{(1)}$, which is already an output of an ϵ -LDP mechanism \mathcal{A} , and does not access the original data d_i .

Hence, the protected inference dataset $\mathcal{D}_{\text{infer}}$ at most consists of all $|\mathcal{D}_{\text{priv}}| \cdot (|\mathcal{D}_{\text{priv}}| - 1)$ data points $\tilde{d}_{i,j}^{(2)}$:

$$\mathcal{D}_{\text{infer}} = \left\{ \tilde{d}_{i,j}^{(2)} \mid \begin{array}{l} i = 1, 2, \dots, |\mathcal{D}_{\text{priv}}|; \\ j = 1, 2, \dots, |\mathcal{D}_{\text{priv}}| - 1 \end{array} \right\}.$$

By Definition 2.3, since the initial mechanism \mathcal{A} satisfies ϵ -LDP, any function g that processes its output without accessing the original data preserves the ϵ -LDP guarantee. The addition of Laplacian noise to $\tilde{d}_i^{(1)}$ is a randomized function g that depends only on $\tilde{d}_i^{(1)}$ and independent random noise $\eta_{i,j}^{(2)}$. Hence, the composite mechanism $g(\mathcal{A}(d_i))$ satisfies:

$$\Pr[g(\mathcal{A}(v_1)) \in \mathcal{T}] \leq e^\epsilon \Pr[g(\mathcal{A}(v_2)) \in \mathcal{T}], \quad (5)$$

for all values v_1, v_2 and all subsets $\mathcal{T} \subseteq \text{Range}(g(\mathcal{A}))$.

Therefore, each data point $\tilde{d}_{i,j}^{(2)}$ in $\mathcal{D}_{\text{infer}}$ satisfies ϵ -LDP due to the post-processing property. The privacy guarantee from the initial noise addition is preserved and the additional noise does not compromise the privacy level. \square

Theorem A.3. *Our noise injection mechanism LDPKiT-Sup satisfies ϵ -LDP.*

Proof. The base noise addition mechanism \mathcal{A} applies the Laplacian mechanism (See Definition 2.2) to obtain the noise-added data point:

$$\tilde{d}_i = d_i + \eta_i,$$

where η_i is a random variable drawn from the Laplacian distribution with probability density function (PDF):

$$L(z, \lambda) = \frac{1}{2\lambda} \exp\left(-\frac{|z|}{\lambda}\right),$$

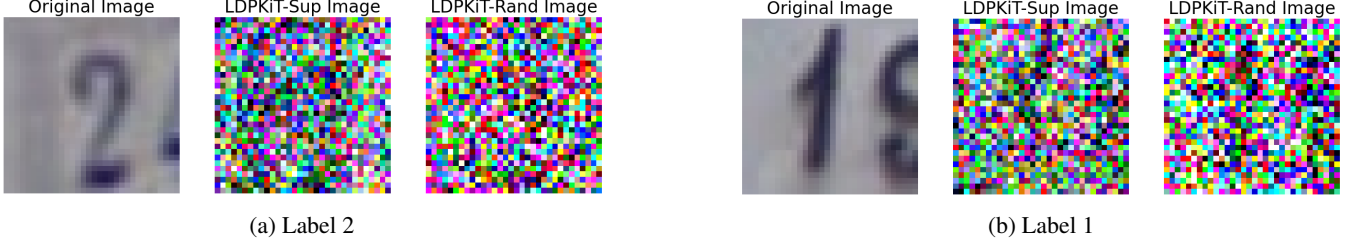


Figure 11: Samples of noised SVHN data with ϵ set to 1.5 (left) and 1.25 (right).

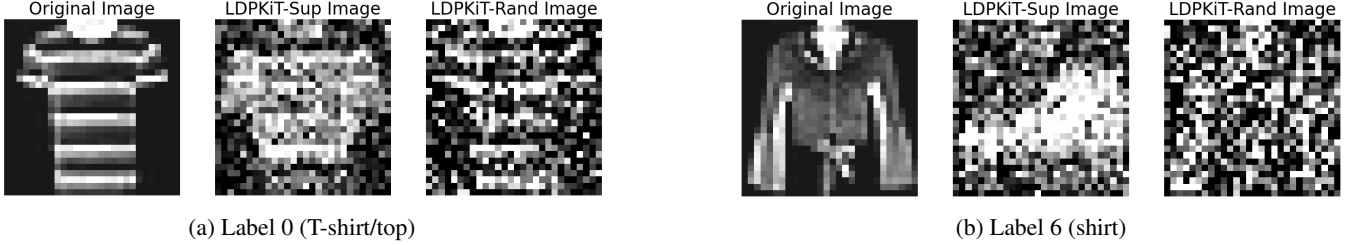


Figure 12: Samples of noised Fashion-MNIST data with ϵ set to 2.0 (left) and 1.5 (right).

and the scaling factor λ is set to $\lambda = \frac{\Delta_f}{\epsilon}$.

By Definition 2.1, the base noise addition mechanism that outputs \tilde{d}_i satisfies ϵ -LDP.

We define a post-processing function g that takes the set of noise-added data points $\{\tilde{d}_1, \tilde{d}_2, \dots, \tilde{d}_{|\mathcal{D}_{\text{priv}}|}\}$ and outputs all possible ordered pairs:

$$\mathcal{D}_{\text{infer}} = g(\{\tilde{d}_i\}) = \{(\tilde{d}_i, \tilde{d}_j) \mid i \neq j, 1 \leq i, j \leq |\mathcal{D}_{\text{priv}}|\}.$$

The total number of data points in $\mathcal{D}_{\text{infer}}$ is $|\mathcal{D}_{\text{priv}}| \cdot (|\mathcal{D}_{\text{priv}}| - 1)$.

By Definition 2.3, if the base noise addition mechanism \mathcal{A} satisfies ϵ -LDP, then any function g applied to its output preserves the ϵ -LDP guarantee.

Since g operates on \tilde{d}_i and does not access the original data d_i , the composite mechanism $g(\mathcal{A}(d_i))$ satisfies:

$$\Pr[g(\mathcal{A}(v_1)) \in \mathcal{T}] \leq e^\epsilon \Pr[g(\mathcal{A}(v_2)) \in \mathcal{T}], \quad (6)$$

for all values v_1, v_2 and all subsets $\mathcal{T} \subseteq \text{Range}(g(\mathcal{A}))$.

Similarly, g does not access the original data d_j since it has base noise that satisfies ϵ -LDP added (i.e., \tilde{d}_j) before composition with \tilde{d}_i . Hence, the privacy guarantee from the initial noise addition in d_j is also not compromised.

Therefore, each data point in $\mathcal{D}_{\text{infer}}$ satisfies ϵ -LDP. The privacy guarantee from the base layer of noise addition is preserved in $\mathcal{D}_{\text{infer}}$ due to the post-processing property. \square

B Hyperparameter choices and dataset preparation

In this section, we document hyperparameter choices and dataset splits for the experiments in Section 4. We use three image benchmarks for evaluation: SVHN with 10 classes of 32x32x3 cropped street view house number images, Fashion-MNIST with 10 classes of 28x28 greyscale fashionable clothing images, and PathMNIST with 9 classes of 28x28x3 medical images of pathology. We train \mathcal{M}_{R} with a learning rate of 0.1 for 200 epochs on Fashion-MNIST and SVHN and 10 epochs on PathMNIST. \mathcal{M}_{R} is trained on 35k data points for Fashion-MNIST, 48,257 data points for SVHN and 89,996 data points for PathMNIST. $\mathcal{D}_{\text{priv}}$ and \mathcal{D}_{val} are split from the remaining data points unseen by \mathcal{M}_{R} , where $\mathcal{D}_{\text{priv}}$ is used to train and evaluate \mathcal{M}_{L} , and \mathcal{D}_{val} is used for pure model generalizability evaluation. Specifically, CIFAR-10 has 15k data points in the candidate pool of $\mathcal{D}_{\text{priv}}$, Fashion-MNIST and SVHN have 25k, and PathMNIST has 10,004. As for \mathcal{D}_{val} , its size is 10k for both CIFAR-10 and Fashion-MNIST, 26,032 for SVHN, and 7,180 for PathMNIST. $\mathcal{D}_{\text{infer}}$ in Sections 4.2 and 4.5 has a size of $|\mathcal{D}_{\text{priv}}| \cdot (|\mathcal{D}_{\text{priv}}| - 1)$ (around 2.2M). In Section 4.4, $|\mathcal{D}_{\text{priv}}|$ is set to 125, 250, 500, 1k and 1.5k, whereas $|\mathcal{D}_{\text{infer}}|$ is set to 15,500, 62,250, 250k and 500k, respectively. In this section, another set of comparison experiment is done with $|\mathcal{D}_{\text{priv}}|$ fixed at 1.5k and $\mathcal{D}_{\text{infer}}$ has a varying size of 250k, 500k, 1M and 2M (i.e., all possible superimposition pairs like Section 4.2). \mathcal{M}_{L} 's learning rate is 0.1 for Fashion-MNIST and 0.001 for SVHN and PathMNIST. The number of training epochs is set to 15 across all the datasets in all scenarios. For the latent space analysis, we train VAE for 200 epochs with a learning rate set to 0.001 for

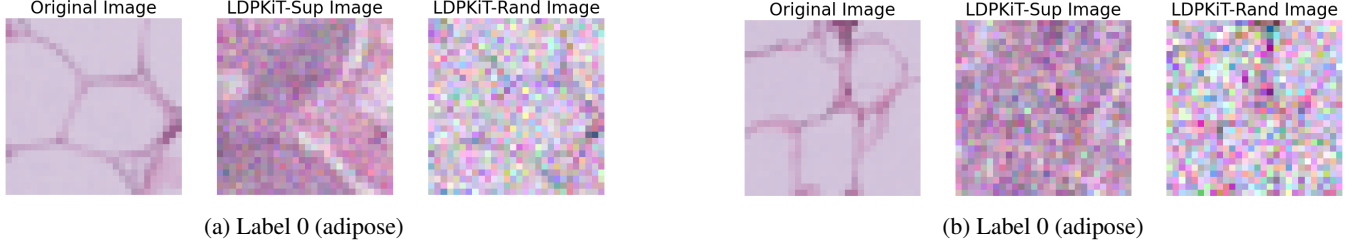


Figure 13: Samples of noised PathMNIST data with ϵ set to 10.0 (left) and 7.0 (right).

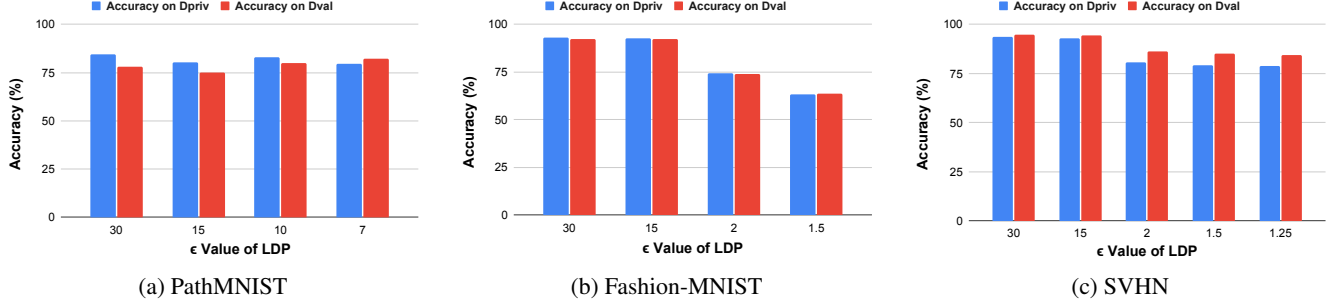


Figure 14: Impact of ϵ values on MobileNetV2 (\mathcal{M}_L)’s accuracies on \mathcal{D}_{priv} versus \mathcal{D}_{val} with LDPKiT-Sup.

Table 5: Final accuracies on \mathcal{D}_{priv} and \mathcal{D}_{val} of SVHN.

Model	ϵ Value	Accuracy on \mathcal{D}_{priv} (%)			Accuracy on \mathcal{D}_{val} (%)		
		SIDP	LDPKiT-Rand	LDPKiT-Sup	SIDP	LDPKiT-Rand	LDPKiT-Sup
ResNet-18	30.0	93.8944 (± 0.7050)	79.4593 (± 0.0448)	93.9556 (± 0.8406)	95.8538 (± 0.0596)	74.6765 (± 4.3553)	95.4970 (± 0.1720)
	15.0	89.4130 (± 0.6467)	90.1259 (± 0.8296)	93.9407 (± 0.6916)	92.7431 (± 0.0944)	89.3243 (± 1.1354)	95.3587 (± 0.1559)
	2.0	21.0657 (± 0.9500)	84.8593 (± 1.7809)	84.6296 (± 1.1161)	29.9870 (± 0.3446)	88.0190 (± 1.4606)	89.1996 (± 0.5978)
	1.5	14.1648 (± 0.8290)	69.6148 (± 1.3020)	84.0815 (± 1.2100)	22.7788 (± 0.3117)	75.9971 (± 1.3721)	88.7301 (± 1.0922)
	1.25	11.8722 (± 0.6702)	54.8593 (± 3.9160)	82.6741 (± 0.8038)	14.8386 (± 0.2211)	63.0220 (± 4.2599)	87.1334 (± 0.7090)
MobileNetV2	30.0	93.8944 (± 0.7050)	59.8370 (± 2.0202)	93.5407 (± 0.9009)	95.8538 (± 0.0596)	57.5527 (± 2.3437)	94.9067 (± 0.1872)
	15.0	89.4130 (± 0.6467)	79.7630 (± 2.4033)	92.9185 (± 0.7444)	92.7431 (± 0.0944)	78.0475 (± 1.7365)	94.5682 (± 0.1779)
	2.0	21.0657 (± 0.9500)	78.9037 (± 1.3885)	80.7481 (± 1.4278)	29.9870 (± 0.3446)	83.5886 (± 1.4901)	86.4235 (± 0.9328)
	1.5	14.1648 (± 0.8290)	62.5185 (± 3.4171)	79.1481 (± 1.0790)	22.7788 (± 0.3117)	70.0202 (± 2.6289)	85.2818 (± 0.8650)
	1.25	11.8722 (± 0.6702)	52.6741 (± 3.6764)	78.8222 (± 1.2728)	14.8386 (± 0.2211)	60.4773 (± 3.6285)	84.2723 (± 0.9145)

SIDP is inference accuracy of ResNet-152 (\mathcal{M}_R) on $\mathcal{D}_{protected}$ without utility trade-off mitigation. The values recorded in parentheses are the standard deviations of the accuracies.

Table 6: Final accuracies on \mathcal{D}_{priv} and \mathcal{D}_{val} of Fashion-MNIST.

Model	ϵ Value	Accuracy on \mathcal{D}_{priv} (%)			Accuracy on \mathcal{D}_{val} (%)		
		SIDP	LDPKiT-Rand	LDPKiT-Sup	SIDP	LDPKiT-Rand	LDPKiT-Sup
ResNet-18	30.0	91.9359 (± 0.3525)	91.6444 (± 0.6625)	93.0222 (± 0.4773)	91.9044 (± 0.1773)	84.0933 (± 1.5904)	92.1978 (± 0.2630)
	15.0	89.0204 (± 0.6521)	91.7185 (± 0.5742)	92.8370 (± 0.3182)	89.0178 (± 0.1862)	89.1944 (± 1.1282)	92.2111 (± 0.2654)
	2.0	28.6944 (± 1.0409)	68.5185 (± 2.4922)	81.7778 (± 2.7049)	28.5200 (± 0.3539)	68.8311 (± 2.7650)	81.6011 (± 2.4087)
	1.5	23.3074 (± 0.8905)	58.0741 (± 4.7133)	73.5037 (± 2.3786)	22.8678 (± 0.1377)	57.9644 (± 4.8297)	73.6200 (± 2.3208)
MobileNetV2	30.0	91.9359 (± 0.3525)	91.6741 (± 0.5390)	92.9750 (± 0.3837)	91.9044 (± 0.1773)	85.5178 (± 1.0833)	92.2800 (± 0.0748)
	15.0	89.0204 (± 0.6521)	89.9556 (± 1.8921)	92.6074 (± 0.4440)	89.0178 (± 0.1862)	86.3111 (± 2.7241)	92.1633 (± 0.1699)
	2.0	28.6944 (± 1.0409)	59.7778 (± 1.9402)	74.3407 (± 2.7658)	28.5200 (± 0.3539)	59.9878 (± 2.0344)	74.0622 (± 3.1608)
	1.5	23.3074 (± 0.8905)	52.0296 (± 4.9529)	63.3852 (± 5.5650)	22.8678 (± 0.1377)	52.3267 (± 4.9828)	63.5922 (± 5.2323)

SIDP is inference accuracy of ResNet-152 (\mathcal{M}_R) on $\mathcal{D}_{protected}$ without utility trade-off mitigation. The values recorded in parentheses are the standard deviations of the accuracies.

Fashion-MNIST. The number of epochs is set to 300 and the

learning rate is 0.0001 for SVHN and PathMNIST.

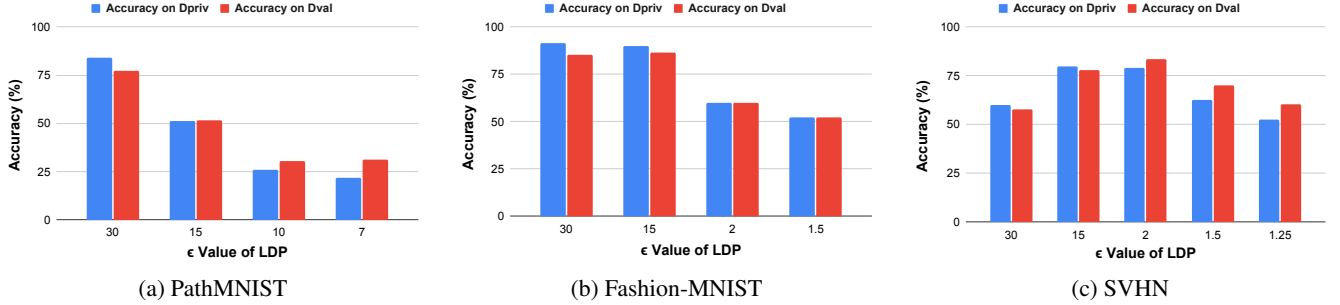


Figure 15: Impact of ϵ values on MobileNetV2 (\mathcal{M}_L)’s accuracies on $\mathcal{D}_{\text{priv}}$ versus \mathcal{D}_{val} with LDPKiT-Rand.

Table 7: Final accuracies on $\mathcal{D}_{\text{priv}}$ and \mathcal{D}_{val} of PathMNIST.

Model	ϵ Value	Accuracy on $\mathcal{D}_{\text{priv}}$ (%)			Accuracy on \mathcal{D}_{val} (%)		
		SIDP	LDPKiT-Rand	LDPKiT-Sup	SIDP	LDPKiT-Rand	LDPKiT-Sup
ResNet-18	30.0	77.6074 (± 0.7298)	84.1333 (± 1.0050)	83.2000 (± 2.5392)	73.9198 (± 0.2818)	78.0718 (± 0.8531)	76.7471 (± 4.6596)
	15.0	47.4315 (± 3.3685)	64.0519 (± 4.6521)	81.5704 (± 2.1463)	46.4268 (± 0.1964)	69.1489 (± 3.5085)	76.7193 (± 1.8324)
	10.0	28.7444 (± 2.9476)	43.9037 (± 3.9903)	82.11 (± 1.8628)	25.8774 (± 0.2397)	43.4478 (± 6.2963)	80.2043 (± 1.5305)
	7.0	22.1759 (± 2.2869)	31.7481 (± 5.6920)	73.29 (± 2.0545)	19.8963 (± 0.2265)	36.2132 (± 6.2276)	76.6543 (± 1.8549)
MobileNetV2	30.0	77.6074 (± 0.7298)	84.1556 (± 0.6137)	84.2889 (± 0.7318)	73.9198 (± 0.2818)	77.3290 (± 1.2886)	77.9944 (± 1.6459)
	15.0	47.4315 (± 3.3685)	51.2519 (± 13.4225)	80.4444 (± 2.2522)	46.4268 (± 0.1964)	51.7394 (± 12.1483)	75.0418 (± 3.5402)
	10.0	28.7444 (± 2.9476)	25.9556 (± 11.1678)	82.8519 (± 1.0540)	25.8774 (± 0.2397)	30.5060 (± 12.7641)	79.9876 (± 1.8408)
	7.0	22.1759 (± 2.2869)	21.8519 (± 11.1653)	79.4370 (± 1.4519)	19.8963 (± 0.2265)	31.3138 (± 13.0969)	82.3398 (± 1.3950)

SIDP is inference accuracy of ResNet-152 (\mathcal{M}_R) on $\mathcal{D}_{\text{protected}}$ without utility trade-off mitigation. The values recorded in parentheses are the standard deviations of the accuracies.

Table 8: Sensitivity Analysis on $|\mathcal{D}_{\text{priv}}|$ and $|\mathcal{D}_{\text{infer}}|$ with ResNet-18 (\mathcal{M}_L) (Continued from Table 3).

Dataset	ϵ	LDPKiT	Accuracy on $\mathcal{D}_{\text{priv}}$ (%)																					
			125				250				500				1k				1.5k					
			$ \mathcal{D}_{\text{priv}} $		$ \mathcal{D}_{\text{infer}} $		$ \mathcal{D}_{\text{priv}} $		$ \mathcal{D}_{\text{infer}} $		$ \mathcal{D}_{\text{priv}} $		$ \mathcal{D}_{\text{infer}} $		$ \mathcal{D}_{\text{priv}} $		$ \mathcal{D}_{\text{infer}} $		$ \mathcal{D}_{\text{priv}} $		$ \mathcal{D}_{\text{infer}} $			
Fashion-MNIST	1.5	Rand	15.73	17.78	23.53	17.49	27.37	45.58	14.11	28.48	49.65	56.41	15.89	30.22	51.16	53.51								
		Sup	18.40	22.27	29.02	21.49	36.91	45.33	22.17	37.16	60.20	65.29	22.34	36.45	58.67	68.66								
SVHN	2.0	Rand	8.40	10.40	10.00	10.00	10.40	56.88	11.40	10.90	56.60	74.13	9.83	12.27	62.48	74.69								
		Sup	10.13	10.13	12.53	10.40	20.13	44.69	10.53	23.07	65.02	71.26	10.04	20.51	66.88	79.94								
SVHN	1.25	Rand	9.60	10.80	6.80	10.30	6.80	19.40	4.85	10.40	18.43	36.18	10.05	9.23	20.18	62.48								
		Sup	9.87	10.27	12.53	9.60	13.27	35.87	10.20	13.50	57.13	65.23	9.76	15.22	57.29	71.90								
Path-MNIST	7.0	Rand	20.27	19.69	17.07	20.91	22.63	36.76	20.71	21.24	38.60	32.67	18.33	19.60	31.42	34.86								
		Sup	30.84	29.02	34.36	30.04	35.38	52.13	28.63	34.82	55.81	65.26	32.02	41.13	59.77	63.99								

C Examples of $\mathcal{D}_{\text{infer}}$ data with LDP noise

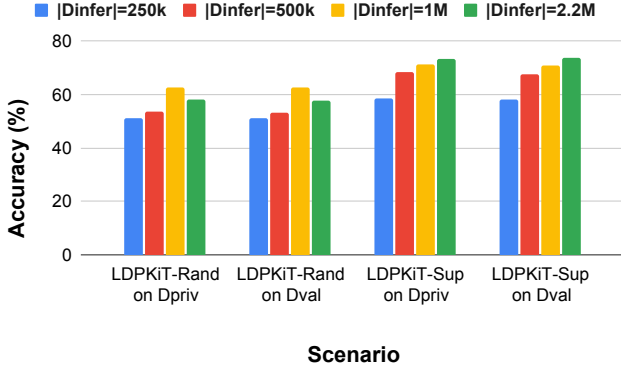
Figures 11, 12, and 13 present comparisons between the original and noised data samples under different levels of ϵ -LDP noise. They also illustrate the impact of our two noise application mechanisms, LDPKiT-Rand and LDPKiT-Sup.

D Additional experimental results

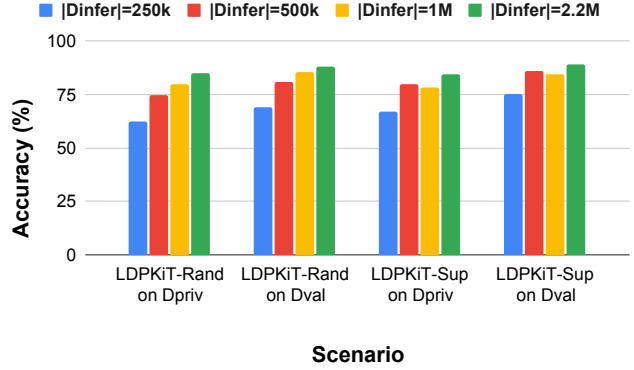
This section is complementary to the evaluation results presented in Section 4.

D.1 Final accuracy on $\mathcal{D}_{\text{priv}}$ and \mathcal{D}_{val}

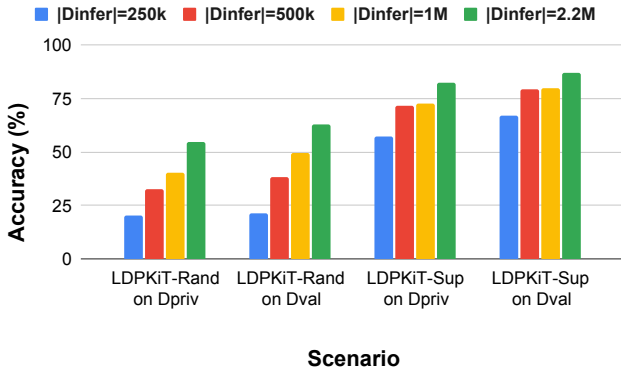
Tables 5, 6 and 7 show the tabulated final accuracies on $\mathcal{D}_{\text{priv}}$ and \mathcal{D}_{val} of SVHN, Fashion-MNIST and SVHN that SIDP, LDPKiT-Rand and LDPKiT-Sup can achieve, which are also presented as bar graphs in Figures 4 and 5 in Section 4.2 and Figures 10, 9, 15 and 14 in Section 4.5 and Appendix D.2. We record the accuracies at the last epoch of training. The results draw the same conclusion as Section 4 that LDPKiT helps offset the accuracy trade-offs brought by LDP noise. The tables also show that LDPKiT can almost always achieve higher inference accuracy than SIDP, but the advantage is less



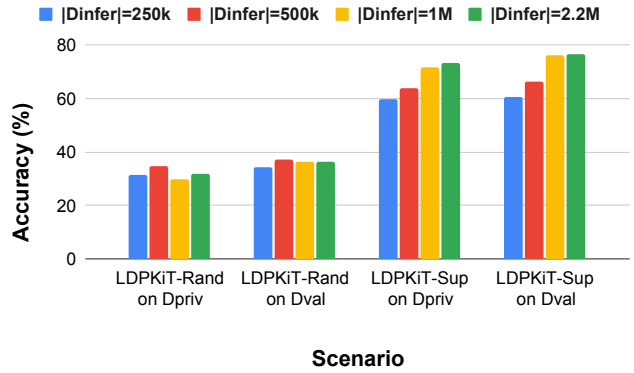
(a) Fashion-MNIST (ε = 1.5)



(b) SVHN (ε = 2.0)



(c) SVHN (ε = 1.25)



(d) PathMNIST (ε = 7.0)

Figure 16: Comparison of ResNet18 (\mathcal{M}_L)’s accuracies on \mathcal{D}_{priv} and \mathcal{D}_{val} with $|\mathcal{D}_{priv}| = 1.5k$ and various $|\mathcal{D}_{infer}|$.

obvious when the least noise is added (*i.e.*, $\epsilon = 30$ or $\epsilon = 15$). However, there is barely privacy protection in these cases, as SIDP accuracies are also very high, indicating a significant information leakage to \mathcal{M}_R . As more LDP noise is added to \mathcal{D}_{priv} to preserve privacy, the gap in utility that LDPKiT provides over SIDP also increases. Therefore, LDPKiT offers greater benefits in regimes with stronger privacy protection and correspondingly more noise.

D.2 Impact of ϵ on MobileNetV2’s Accuracies on \mathcal{D}_{priv} versus \mathcal{D}_{val}

We observe the same trend in Figures 14 and 15 as per discussion in Section 4.5 with MobileNetV2 across all three benchmarks.

D.3 Additional Dataset Size Sensitivity Analysis

The results in this section are complementary to the discussion in Section 4.4. Table 8 shows the impact of $|\mathcal{D}_{infer}|$ and $|\mathcal{D}_{priv}|$ with other ϵ values. All the additional results align with the

conclusions drawn from Table 3. Figure 16 demonstrates the impact of $|\mathcal{D}_{infer}|$ with other ϵ values on the three image benchmarks. The takeaway aligns with the conclusion drawn from Figure 8 that although larger \mathcal{D}_{infer} helps model training and leads to higher accuracies, LDPKiT can already achieve satisfactory accuracies on \mathcal{D}_{priv} and \mathcal{D}_{val} when $|\mathcal{D}_{infer}|$ is 500k. The main takeaway aligns with the discussion in Section 4. LDPKiT’s accuracies increase as $|\mathcal{D}_{infer}|$ increases; however, the improvement becomes minor with larger \mathcal{D}_{infer} and the accuracies are sufficiently high when $|\mathcal{D}_{infer}|$ is 500k. Furthermore, LDPKiT is less sensitive to $|\mathcal{D}_{priv}|$, so LDPKiT can achieve decent accuracies when the user owns a relatively smaller \mathcal{D}_{priv} .

D.4 Additional results of latent space analysis

Apart from the latent space discussion in Section 4.3, we show more analyses of other class triplets and datasets in this section.

Figure 17 presents an example of latent space visualization. Our primary observation is that, regardless of the base image’s class, \mathcal{D}_{infer} generated by LDPKiT-Sup is consistently

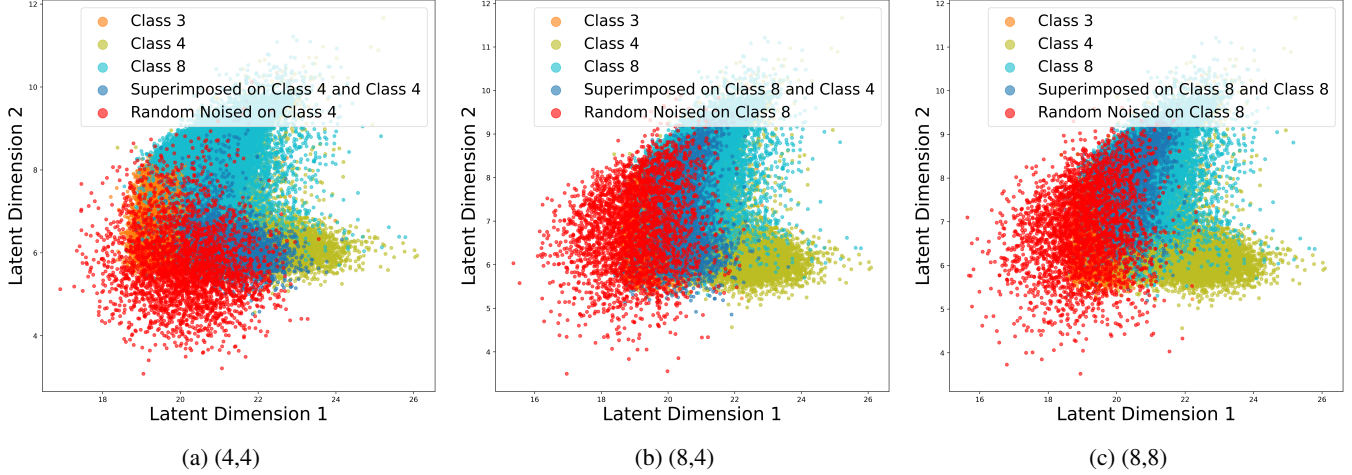


Figure 17: Latent space plots of PathMNIST class triplets (C3-lymphocytes, C4-mucus, C8-colorectal adenocarcinoma epithelium) and privacy-protected noisy data clusters generated with LDPKiT-Rand and LDPKiT-Sup ($\epsilon = 7.0$).

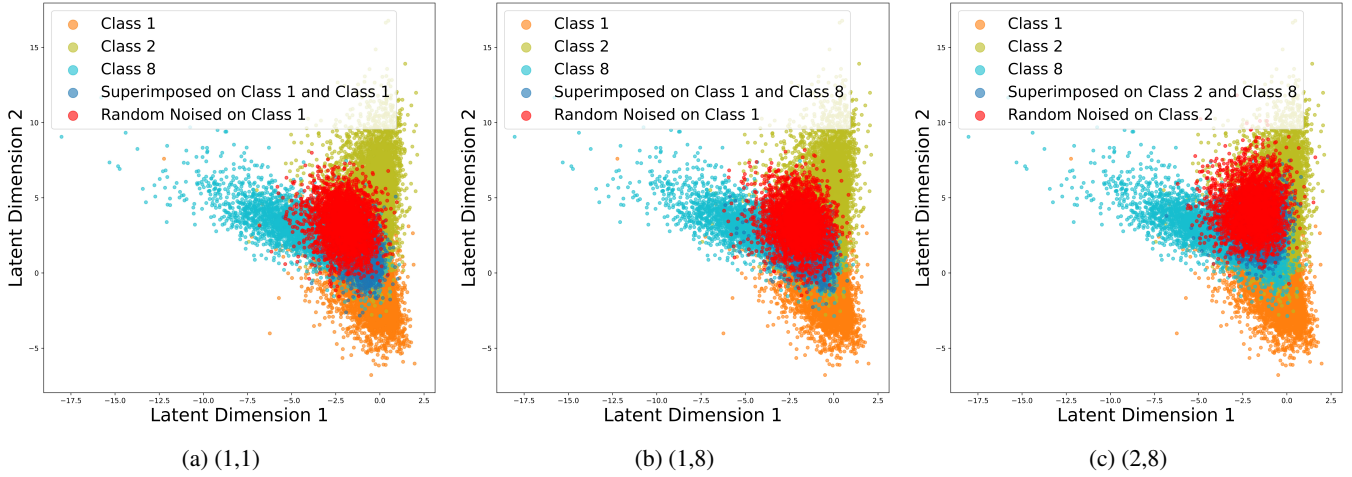


Figure 18: Latent space plots of SVHN class triplets (C1, C2, C8) and privacy-protected noisy data clusters generated with LDPKiT-Rand and LDPKiT-Sup ($\epsilon = 2.0$).

Table 9: Euclidean distances between centroids of clusters shown in Figure 17 on PathMNIST.

Figure	Strategy	Class(es)	$d(C_N, C_3)$	$d(C_N, C_4)$	$d(C_N, C_8)$
17a	LDPKiT-Sup	(4,4)	1.9453	1.5981	2.5698
	LDPKiT-Rand	4	1.8724	2.5812	3.3226
17b	LDPKiT-Sup	(8,4)	1.4984	2.1860	2.0151
	LDPKiT-Rand	8	1.6577	3.3427	3.0580
17c	LDPKiT-Sup	(8,8)	1.6301	2.4562	1.5323
	LDPKiT-Rand	8	1.6407	3.3359	3.0413

$d(C_N, C_X)$ is the Euclidean distance between the centroids of the noisy data cluster and the Class X cluster.

more accurate compared to LDPKiT-Rand. As demonstrated in Figures 17a and 17c, LDPKiT-Sup consistently forms a

Table 10: Euclidean distances between centroids of clusters shown in Figure 18 on SVHN.

Figure	Strategy	Class(es)	$d(C_N, C_1)$	$d(C_N, C_2)$	$d(C_N, C_8)$
18a	LDPKiT-Sup	(1,1)	2.6877	3.1031	3.2987
	LDPKiT-Rand	1	4.4212	3.0084	3.1381
18b	LDPKiT-Sup	(1,8)	2.8854	3.0853	2.9836
	LDPKiT-Rand	1	4.4242	3.0094	3.1386
18c	LDPKiT-Sup	(2,8)	3.8513	2.5689	3.1065
	LDPKiT-Rand	2	5.2321	3.0173	3.5754

$d(C_N, C_X)$ is the Euclidean distance between the centroids of the noisy data cluster and the Class X cluster.

cluster whose distribution is closer to the target class distribution than LDPKiT-Rand. Furthermore, Figure 17b shows

Table 11: Normalized Zest distance results with l_1 distance metric on \mathcal{M}_R and \mathcal{M}_L .

\mathcal{M}_R	\mathcal{M}_L	Mechanism	Fashion-MNIST		SVHN		PathMNIST	
			$\epsilon=2.0$	$\epsilon=1.5$	$\epsilon=1.5$	$\epsilon=1.25$	$\epsilon=10.0$	$\epsilon=7.0$
ResNet-152	ResNet-18	LDPKiT-Sup	1.5904	1.7448	1.1977	1.2286	10.2420	10.2548
		LDPKiT-Rand	1.9605	2.0126	1.6078	1.6785	10.3160	9.5630
	MobileNetV2	LDPKiT-Sup	4.41e+07	8.11e+07	1.2175	1.2595	INF	INF
		LDPKiT-Rand	431.5359	1.5733	1.3581	1.2679	INF	INF

An adversarial model extraction attack is detected if the normalized Zest distance is smaller than 1.0.

Table 12: Normalized Zest distance results with l_2 distance metric on \mathcal{M}_R and \mathcal{M}_L .

\mathcal{M}_R	\mathcal{M}_L	Mechanism	Fashion-MNIST		SVHN		PathMNIST	
			$\epsilon=2.0$	$\epsilon=1.5$	$\epsilon=1.5$	$\epsilon=1.25$	$\epsilon=10.0$	$\epsilon=7.0$
ResNet-152	ResNet-18	LDPKiT-Sup	1.5760	1.7553	1.1753	1.1899	10.2420	10.2548
		LDPKiT-Rand	1.8586	2.0222	1.5914	1.8143	10.3160	9.5630
	MobileNetV2	LDPKiT-Sup	4.16E+08	9.12E+08	1.1692	1.1756	INF	INF
		LDPKiT-Rand	3.60E+03	1.5568	1.4110	1.3631	INF	INF

An adversarial model extraction attack is detected if the normalized Zest distance is smaller than 1.0.

that LDPKiT-Sup’s cluster is positioned between the clusters of Class 4 and Class 8, while LDPKiT-Rand, despite being generated on Class 8 data, remains farther from the correct distribution. We validate these observations by calculating the Euclidean distances between cluster centroids. As shown in Table 9, while both LDPKiT-Sup and LDPKiT-Rand clusters are naturally closer to the Class 3 distribution, LDPKiT-Sup can generate a \mathcal{D}_{infer} cluster that aligns more closely with the target class of the base image. For instance, LDPKiT-Sup’s cluster is closest to Class 4 when superimposition is applied on two Class 4 data. In contrast, LDPKiT-Rand remains relatively static, always nearest to the Class 3 distribution regardless of the base image’s class. The results of SVHN in Figure 18 and Table 10 also align with other datasets. Visually, LDPKiT-Rand’s distribution remains relatively more static than LDPKiT-Sup, regardless of the label of the base image. LDPKiT-Sup, on the other hand, moves closer to the target cluster(s) of the two superimposed images.

E Model extraction attack detection with Zest

This section discusses more details of Zest [65]’s usage and results.

E.1 Steps of model extraction detection

According to the Zest paper [65], we detect model extraction in the following steps:

1. Calculate the Zest distance between the two models to compare, *i.e.*, $D_z(\mathcal{M}_R, \mathcal{M}_L)$, where \mathcal{M}_L is trained on the entire data split of the noisy \mathcal{D}_{priv} , disjunctive to \mathcal{M}_R ’s training dataset.
2. Calculate a reference distance by computing the average distance between five pairs of the victim and extracted models, denoted as \mathcal{M}_V and \mathcal{M}_E , where \mathcal{M}_E are generated by training on \mathcal{M}_V ’s labeled training dataset, *i.e.*,

$$D_{ref} = \frac{1}{5} \sum_{i=1}^5 D_z(\mathcal{M}_{Vi}, \mathcal{M}_{Ei}).$$

Here, \mathcal{M}_V has the same model architecture as \mathcal{M}_R , and \mathcal{M}_E has the same model architecture as \mathcal{M}_L , but trained on the same dataset as \mathcal{M}_V , rather than the noisy \mathcal{D}_{priv} .

3. Calculate the normalized Zest distance, *i.e.*, $\overline{D}_z = \frac{D_z}{D_{ref}}$.
4. Determine the existence of model extraction by comparing \overline{D}_z with *threshold* 1.

$\overline{D}_z < 1$ indicates \mathcal{M}_R and \mathcal{M}_L are similar models and model extraction occurs.

$\overline{D}_z > 1$ indicates \mathcal{M}_R and \mathcal{M}_L are dissimilar, and thus no model extraction attack exists.

Table 13: Normalized Zest distance results with l_∞ distance metric on \mathcal{M}_R and \mathcal{M}_L .

\mathcal{M}_R	\mathcal{M}_L	Mechanism	Fashion-MNIST		SVHN		PathMNIST	
			$\epsilon=2.0$	$\epsilon=1.5$	$\epsilon=1.5$	$\epsilon=1.25$	$\epsilon=10.0$	$\epsilon=7.0$
ResNet-152	ResNet-18	LDPKiT-Sup	1.9396	2.2138	1.1204	1.1532	9.1840	9.3871
		LDPKiT-Rand	2.1970	2.1826	1.5332	2.2498	9.2258	9.5491
	MobileNetV2	LDPKiT-Sup	1.67E+09	5.86E+09	1.1469	1.1004	INF	INF
		LDPKiT-Rand	1.04E+04	1.6815	1.5919	1.7202	INF	INF

An adversarial model extraction attack is detected if the normalized Zest distance is smaller than 1.0.

E.2 Zest distances supplementary results

We show the Cosine Distance measurement in the main paper as it is the most accurate metric [65]. We provide additional experimental results with l_1 , l_2 and l_∞ distance metrics supported by Zest in Tables 11, 12 and 13 on \mathcal{M}_L generated from Section 4.2. The results draw the same conclusion as Section 6.1 that the type of knowledge distillation in LDP-KiT does not construct an adversarial model extraction attack quantitatively.